ASYMMETRICALLY THYRISTOR CONTROLLED REACTOR FOR STATIC VAR SYSTEM

A Thesis Submitted

In Partial Fulfilment of the Requirements

for the degree of

MASTER OF TECHNOLOGY

by

PANNA LAL BISWAS

to the

DEPARTMENT OF ELECTRICAL ENGINEERING
INDIAN INSTITUTE OF TECHNOLOGY, KANPUR

March, 1993

CERTIFICATE

It is certified that the work contained in this thesis entitled "ASYMMETRICALLY THYRISTOR CONTROLLED REACTOR FOR STATIC VAR SYSTEM" by Panna Lal Biswas has been carried out under our supervision and that this work has not been submitted elsewhere for a degree.

Dr. Sachchidanand
Professor
Dept. of Electrical Engg
Indian Institute of Technology
Kanpur, India

(On long leave)
Dr R. K. Varma
Assistant Professor
Dept. of Electrical Engg.
Indian Institute of Technology
Kanpur, India

9th March, 1993.

CERTIFICATE

It is certified that the work contained in this thesis entitled "ASYMMETRICALLY THYRISTOR CONTROLLED REACTOR FOR STATIC VAR SYSTEM" by Panna Lal Biswas has been carried out under our supervision and that this work has not been submitted elsewhere for a degree

Sachchidanand

Dr. Sachchidanand
Professor
Dept. of Electrical Engg.
Indian Institute of Technology
Kanpur, India

(On long leave)
Dr. R. K. Varma
Assistant Professor
Dept of Electrical Engg.
Indian Institute of Technology
Kanpur, India

9th March, 1993.

DEDICATED

TO MY

PARENTS

ACKNOWLEDGEMENTS

With a profound sense of gratitude I express my sincere thanks to my teachers and guides Dr. Sachchidanand and Dr R.K. Varma for their invaluable guidance throughout the course of this work. Only because of their patient guidance and encouragement, I have been able to complete this work they taught me various courses in power systems and are always a source of inspiration to me I humbly express my indebtness for all that they have done for me during my stay here

I am extremely thankful to Dr S.S. Prabhu for the help he has extended to me to complete this work

I am greatful to Dr. S.R. Doradla and Dr. G.K Dubey for having taught me various courses.

I am extemely thankful to Mr. M.K. Narayan for his immense contribution during the thesis prepartion.

I am thankful to Mr.Santosh Kumar, Mr. Rajkumar Singh, Mr Vimal Modi, Mr. Biswarup Das, Mr. B S. Misra and Mr. Shivanand for their help at various stages of this work. Their contribution to my work is respectfully acknowledged.

It is a matter of great pleasure to work in the splendid company of my friends Biswal, Ajay and Brijesh . I express my sincere thanks to all of them on this ocassion.

I thank to Km Chandana and Km. Vandana for their constant inspiration during my stay at I.I.T. Kanpur.

I thank Mr. L S. Bajpai for his skillful typing of this thesis. I thank to all others who have helped me in any way.

I.I.T.Kanpur,
March, 1993.

PANNA LAL BISWAS

TABLE OF CONTENTS

LIST OF FIGURE

ABSTRACT

Asymmetrically triggered Thyristor Controlled Reactor(TCR) has been suggested as a possible alternative to the conventional Thyristor Controlled Reactor(TCR) in Static Var Systems. This thesis deals with the detailed investigation of asymmetrically triggered TCR.

Steady State analysis of the asymmetrically triggered TCR has been carried out in relation to input current, output voltage, harmonic contents in various quantities and rective power generation capability in all the three possible modes of operation. A comparative evaluation of this TCR and conventional TCR has been made. It has been observed that, from device point of view, the asymmetrically triggered TCR is decidedly better than the conventional one as it requires thyristor of lower current rating and inductor of smaller size for the same reactive power. A case study, ignoring transients, has been undertaken in order to assess the efficacy of this TCR in SVS applications.

CHAPTER - 1

INTRODUCTION

1.1 GENERAL

Reactive power compensation plays an important role in the operation of power transmission system. The reactive power requirement has traditionally been met through shunt capacitor, shunt reactor, synchronous condenser etc. However, all these devices suffer from certain limitations of either range of control, flexibility or speed. With the advent of thyristor, a fast and smooth control of reactive power has been made possible through Static Var System [1,2,3]. The flexibility in control of SVS has made it attractive not only for bus voltage control but also for improving system stability through damping of power system oscillations.

Static Var System comprises of thryistor controlled reactor together with either fixed capacitor or thyristor switched capacitor. The thyristor control enables a smooth and fast control of reactive power. Although SVS technology has reached a fairly matured stage, attempts are continuously being made to improve the performance through use of alternate power semiconductor devices or thyristor control techniques.

1.2 REVIEW OF LITERATURE

Reactive compensation in power system has traditionally been achieved through switched shunt reactor, switched shunt capacitor, series capacitor, synchronous condenser, saturable reactor, thyristor controlled reactor(TCR)and thyristor switched capacitor(TSC). These compensating devices can be classified into two categories

(a) Internally controlled devices

(b) Externally controlled devices

Switched shunt reactor, switched shunt capacitor, series capacitor, sychronous condenser and saturable reactor fall in the first category, where there is an inherent limitation of flexibility of control On the contrary, thyristor controlled devices (TCR and TSC) which are externally controlled devices permit flexibility in control and hence are better suited for most applications [4-8]. Static Var Systems enable smooth and fast control of reactive power over the complete range from inductive to capacitive. The two most commercially used configurations of SVS are :

i) Fixed capacitor, thyristor controlled reactor (FC-TCR)

ii) Thyristor switched capacitor, thyristor controlled reactor (TSC-TCR)

Fig. 1 1 and Fig 1 2 show both these types of SVS configurations. Steady state characteristic of both the compensators are identical for small voltage perturbations [4]

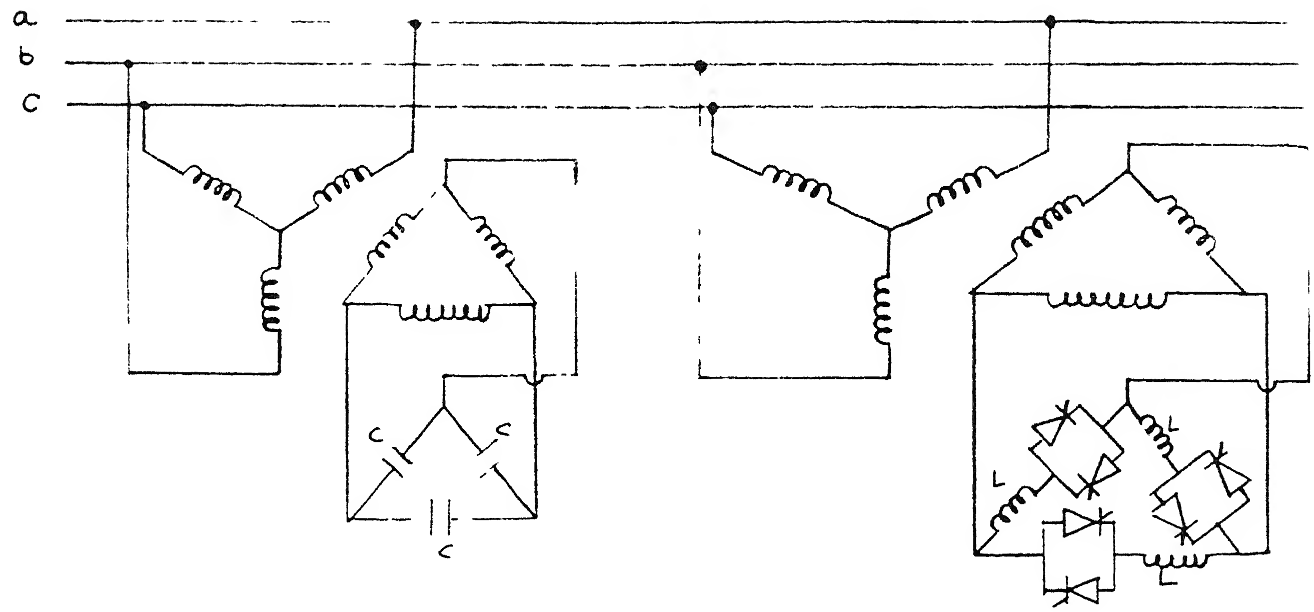

FIG - 11 : FC TCR COFIGURATION

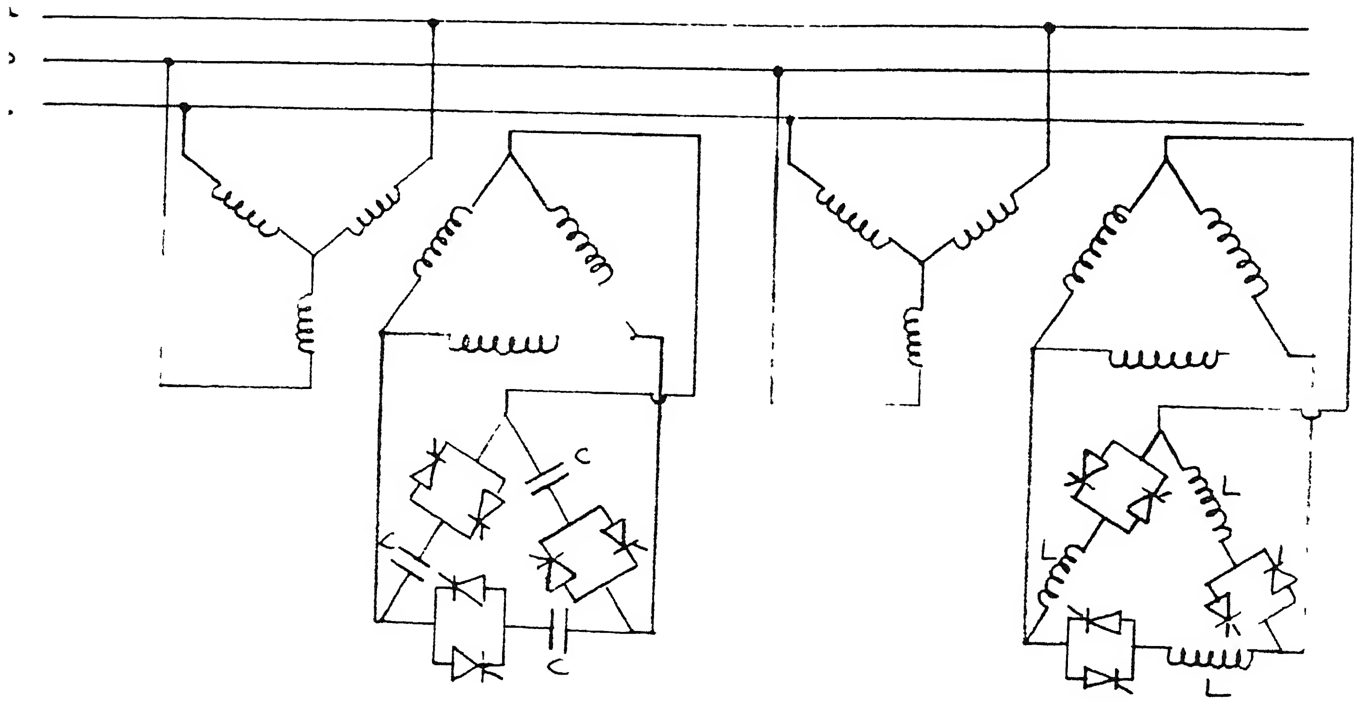

FIG - 12 : TSC TCR CONFIGURATION

The performance of TSC-TCR is superior under large system disturbances. Moreover, TSC-TCR is characterized by low losses and reduced harmonic content [1]

Exploiting the development in power semiconductor devices, the TCR configuration has also been proposed with gate-turn-off thyristors (GTO) [10,12] The basic advantage which is expected with the use of GTO is better flexibility in control with selective elimination [4,7,10] of harmonics

In addition to the above, alternate control strategies for the thyristor controlled reactor also have been proposed with the view point of improved system performance. In this context, the design of thyristor controlled reactor has been proposed by Hammad et al [5-6], which allows for an increased control range, minimized harmonic generation and reduction in voltage stresses on the valves. Two new schemes of SVS have also been proposed, one is "Power Doubling" VAR generator [1], and other is SVS utilizing superconducting coil [8].

An asymmetrically triggered phase controlled reactor has been proposed as a potential alternative to conventional Thyristor Controlled Reactor [9,10] This proposed scheme uses only one inductor to achieve the desired control of reactive power, as compared to three inductors used in conventional TCR scheme Although this seems to be quite attractive since it will result in significant cost reduction, a detailed technical performance evaluation is however necessary with regards to steady and

transient operation, harmonic generation and range of reactive power control In this thesis some of these aspects of asymmetrically triggered TCR have been examined.

1.3 OBJECTIVE AND SCOPE OF THE THESIS

This thesis is mainly concerned with the analysis of asymmetrically triggered TCR to explore the possibility of its use in Static VAR System as alternative to conventional TCR. In this context, the main objectives of the thesis are ·

1. To analyse the asymmetrically triggered TCR under steady statewith regards to input current, output voltage and output current.
2. Performance evaluation as regards harmonic generation and range of reactive power control.
3. To study the effectiveness of asymmetrically triggered TCR in Static VAR System applications.

1.4 OUTLINE OF THE THESIS

Chapter 2 undertakes the steady state analysis of the unsymmetrically triggered TCR. The general analysis for all three modes, with regards to input phase current, output current and output voltage, has been carried out The expressions for phase input current and output voltage have been derived.

In Chapter 3 harmonic analysis and reactive power study have been undertaken. The harmonics in input current, output voltage and output current, in all the three modes, have been evaluated

The reactive power generation based on fundamental component analysis has been evaluated.

In Chapter 4, asymmetrically triggered TCR has been used in Static VAR compensator The voltage control capability of thhis new TCR has been investigated through simulation.

CHAPTER - 2

STEADY STATE ANALYSIS OF AN ASYMMETRICALLY TRIGGERED THYRISTOR CONTROLLED REACTOR

The steady state operation of a thyristor controlled reactor (TCR) based on asymmetrical firing is analysed in this chapter. Different modes of operation have been identified. The TCR performance has been analysed by deriving steady state expressions for currents and voltages.

2.1 THYRISTOR CONTROLLED REACTOR OPERATION

The configuration of the thyristor controlled reactor is shown in Fig. 2.1. This shows a reactor (L) connected at the output terminal of a conventional three phase thyristor bridge which is fed from a balanced three phase supply (v_a, v_b, v_c). L_s represents the leakage inductance of the transformer. In the conventional three phase converter bridge operation or conventional thyristor controlled reactor, the thyristors 1 through 6 are fired with the same delay angle α measured with respect to the positive going zero crossing of the respective commutation voltage. The asymmetrical firing of the valves considered here involves firing of the thyristor in the upper valve group (1,3,5) with a delay angle α_P and the thyristor in the lower valve group (2,4,6) with a delay angle α_N such that

$$\alpha_P + \alpha_N = 180^\circ \tag{2.1}$$

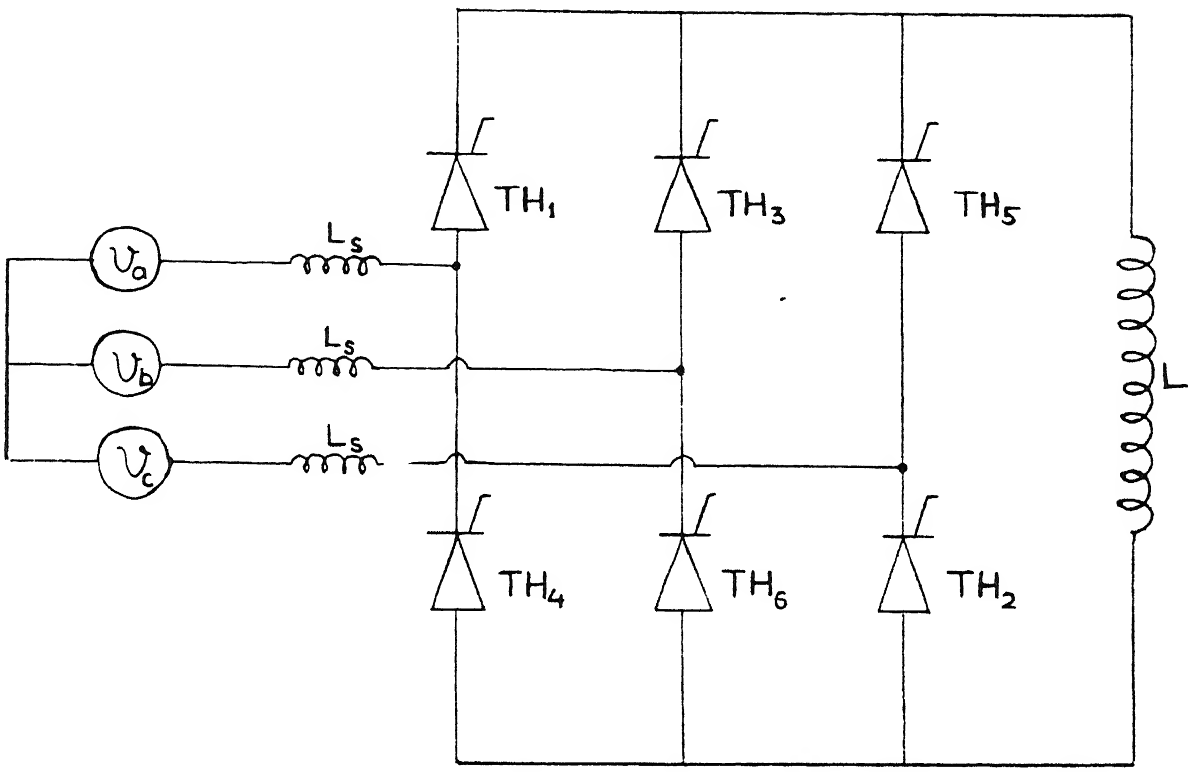

FIG.2.1 TCR CONFIGURATION

Under the asymmetrical firing scheme, the position of firing pulses for various valves is shown in Fig. 2.2 for different values of α_P in the range 0° to 180°. Based on this the valve conduction pattern over one cycle can be established as given in Table 2.1.

With the asymmetrical firing the TCR operation can be explained with the help of Fig. 2.3. which shows the output voltage waveform. The reference $\omega t = 0$ has been indicated in the figure. Firing angle (α_P) is 30° and L_s is assumed to be zero. For $0^\circ \leq \omega t \leq 60^\circ$, valves 4 and 5 are conducting, as indicated in Table 2.1. Therefore, voltage v_{ca} appears across the inductance (L). For $120^\circ \leq \omega t \leq 180^\circ$, valves 1 and 6 are conducting and hence the output voltage is v_{ab}. Between $240^\circ \leq \omega t \leq 300^\circ$, conducting valves are 2 and 3, and the output voltage is v_{bc}. In other intervals both the thyristors of the same limb (1,4 or 2.5 or 3,6) are conducting and as a result output voltage is zero. The output voltage waveforms for various values of α_P in the range 0° to 180° are shown in Fig. 2.4.

As can be observed from Fig. 2.4 the asymmetrically triggered three phase converter has an alternating output voltage waveform and hence the average dc output voltage is zero for any value of α_P and α_N. As α_P, and consequently α_N is varied, it can also be seen that the number of pulses appearing in the output voltage waveform changes from 3 pulses (in the intervals $0^\circ \leq \alpha_P \leq 60^\circ$ and $120^\circ \leq \alpha_P \leq 180^\circ$) and 6 pulses (in the interval $60^\circ \leq \alpha_P \leq 120^\circ$) Based on this, it is evident that converter

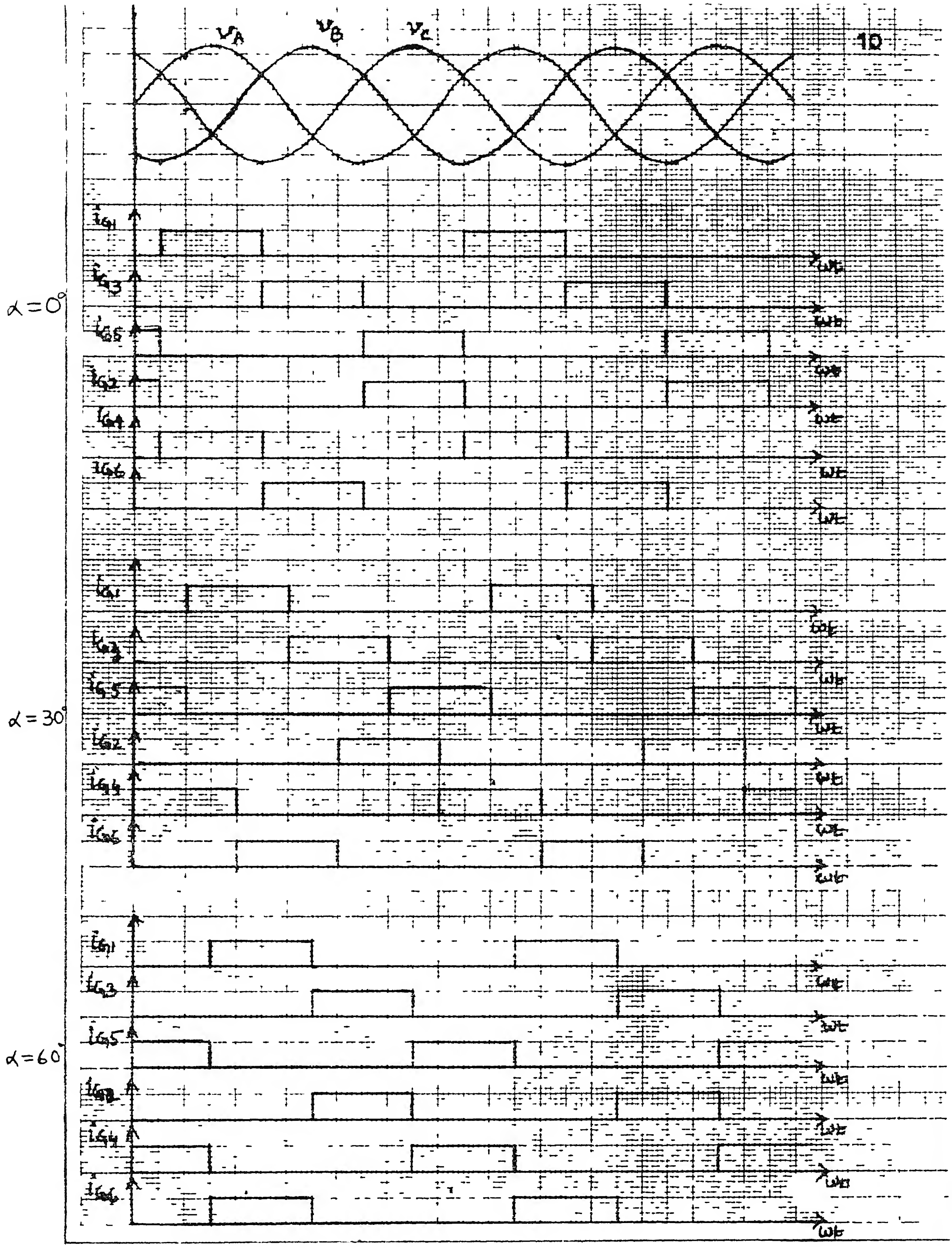

FIG. 22 FIRING PULSE FOR DIFFERENT VALVES

11

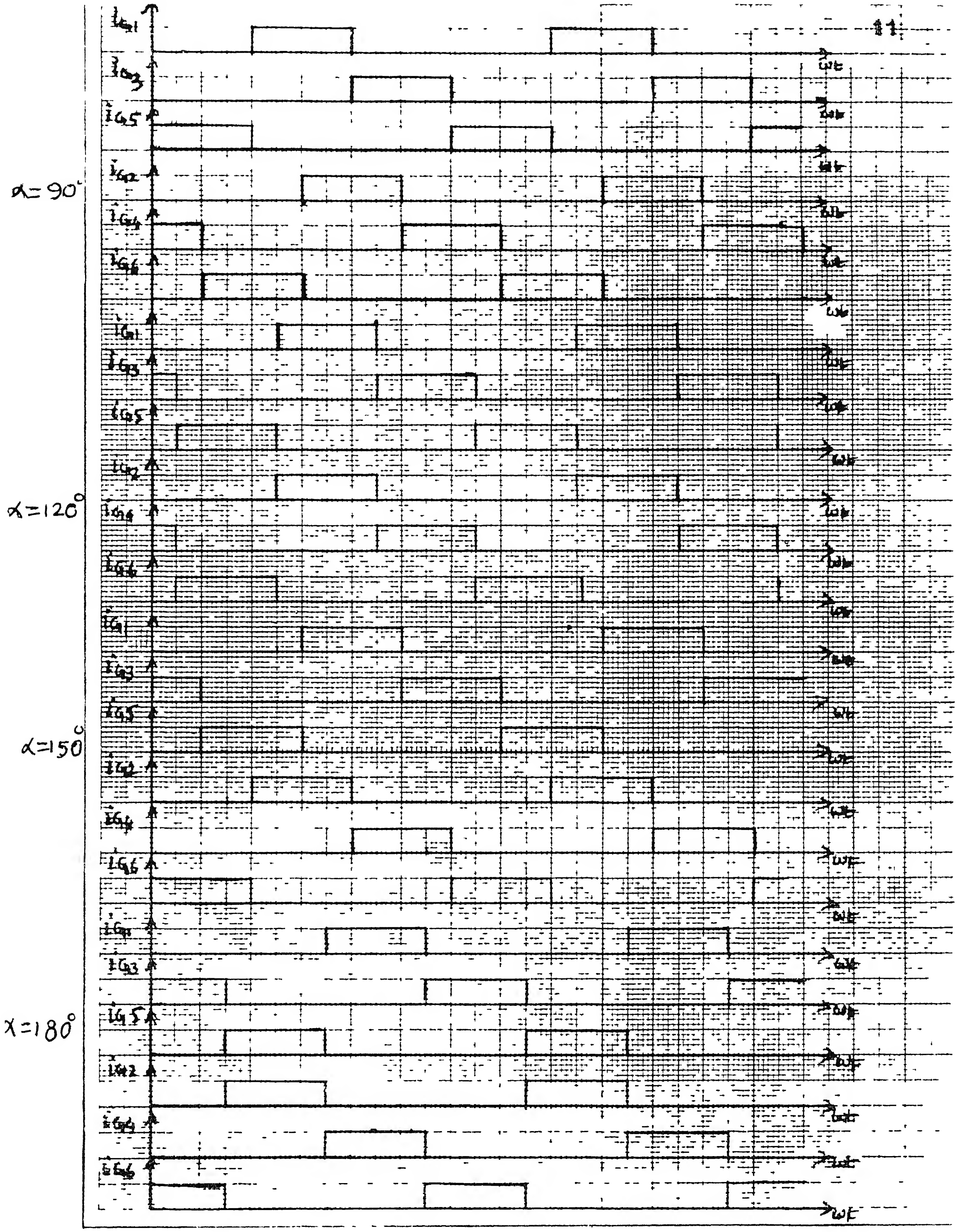

$\alpha = 90°$
$\alpha = 120°$
$\alpha = 150°$
$\alpha = 180°$
i_{G1}
i_{G3}
i_{G5}
i_{G2}
i_{G4}
i_{G6}
ωt

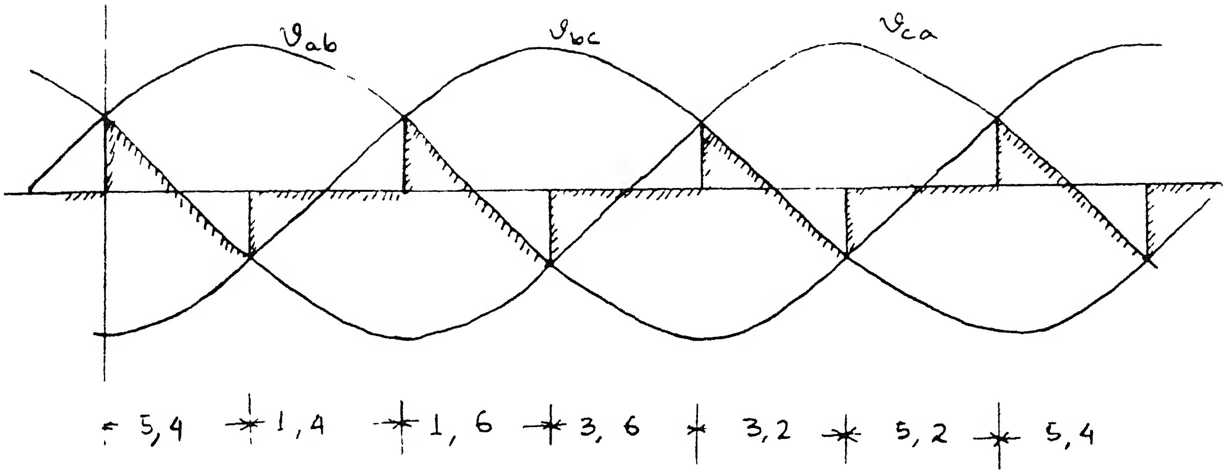

FIG 23 : OUTPUT VOLTAGE SUPERIMPOSED ON INPUT VOLTAGE FOR $\alpha = 30°$

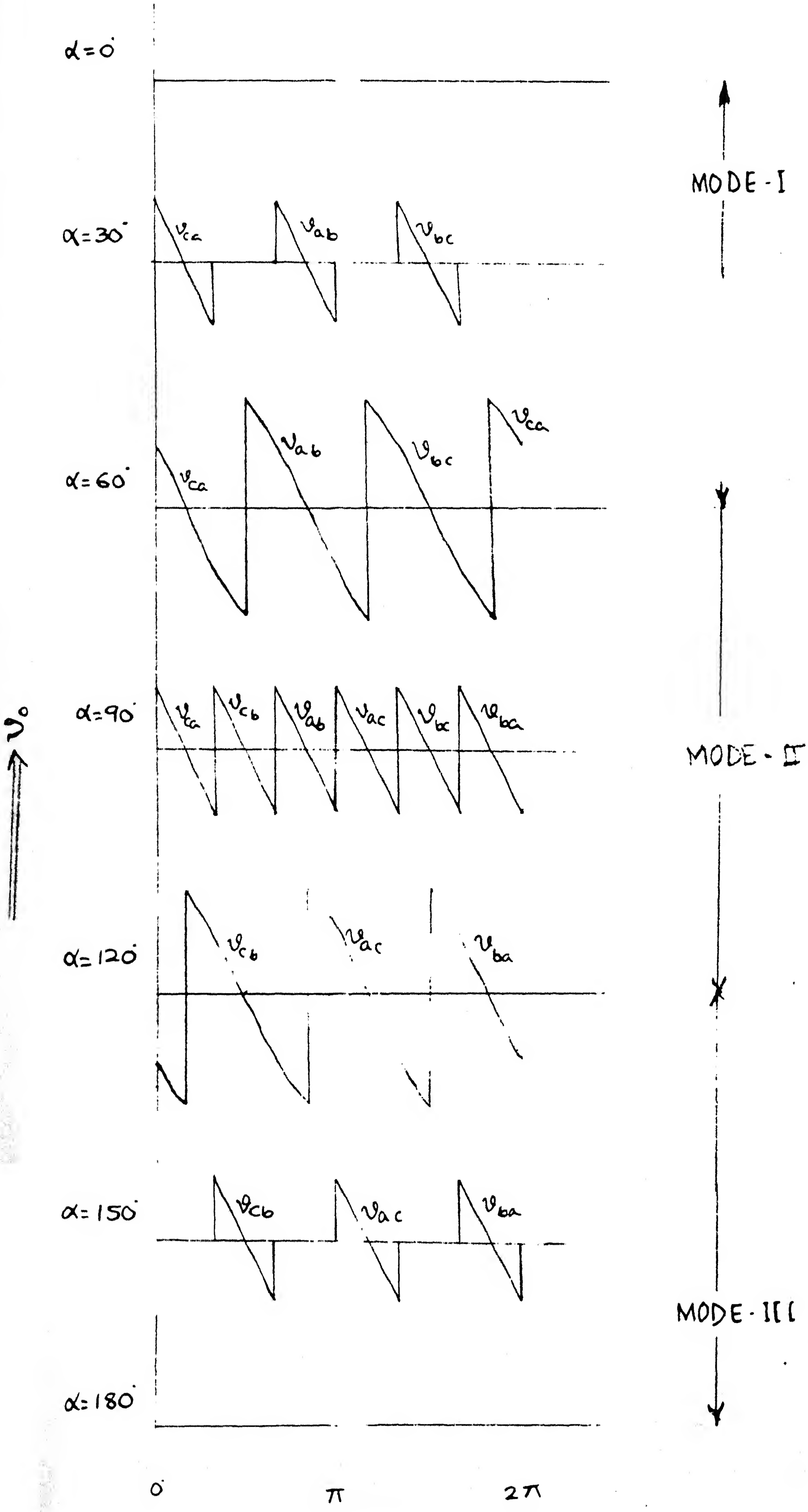

FIG 2.4 : OUTPUT VOLTAGE WAVEFORM IN ALL THREE MODES

undergoes three different modes of operation as α_p is varied form 0° to 180°. These modes are

$$\text{MODE I} : 0^\circ \le \alpha_p \le 60^\circ$$

$$\text{MODE II} : 60^\circ \le \alpha_p \le 120^\circ$$

$$\text{MODE III} : 120^\circ \le \alpha_p \le 180^\circ$$

The steady state operation of TCR is analysed for all the three modes of operation. To simplify the analysis, the following assumptions are made:

(i) Thyristors are treated as ideal switches.

(ii) The inductor (L) is assumed to be ideal.

(iii) The source voltages are assumed to be sinusoidal and balanced, i.e.

$$v_a = V_m \sin(\omega t) \qquad 2.2(a)$$

$$v_b = V_m \sin(\omega t - 120^\circ) \qquad 2.2(b)$$

$$v_c = V_m \sin(\omega t + 120^\circ) \qquad 2.2(c)$$

The line voltages are

$$v_{ab} = -v_{ba} = \sqrt{3}\, V_m \sin(\omega t + 30^\circ) \qquad 2.3(a)$$

$$v_{bc} = -v_{cb} = \sqrt{3}\, V_m \sin(\omega t - 90^\circ) \qquad 2.3(b)$$

$$v_{ca} = -v_{ac} = \sqrt{3}\, V_m \sin(\omega t + 150^\circ) \qquad 2.3(c)$$

The TCR operation is analysed both with and without source inductance L_s. For the sake of convenience in the analysis to follow α_p is designated as α.

2.2 TCR OPERATION WITHOUT SOURCE INDUCTANCE (L_s)

2.2.1 Input Current in Mode I Operation

From the voltage waveform shown in Fig. 2.4 it can be seen that in mode I, the output voltage will have only three pulses corresponding to v_{ca}, v_{ab} and v_{bc}. Each of these line voltage appear for a duration of 2α. This is illustrated in Fig. 2.5 which also shows the nature of input phase A current. In Fig. 2.5 it is considered that the zero crossover of voltages v_{ca}, v_{ab} and v_{bc} occur at $\omega t = 30^\circ$, $\omega t = 150^\circ$ and $\omega t = 270^\circ$ respectively. From this it can be observed, in general, that for any firing angle α in mode I the output voltage equals v_{ca} from $\omega t = (30^\circ - \alpha)$ to $\omega t = (30^\circ + \alpha)$, equals v_{ab} from $\omega t = (150^\circ - \alpha)$ to $\omega t = (150^\circ + \alpha)$ and equals v_{bc} from $\omega t = (270^\circ - \alpha)$ to $\omega t = (270^\circ + \alpha)$. In any intermediate time period the output voltage is zero. Based on this, one complete cycle can be subdivided in three regions, for the purpose of analysis, as follows

Region 1 : $(30^\circ - \alpha) \le \omega t \le (30^\circ + \alpha)$

Region 2 : $(150^\circ - \alpha) \le \omega t \le (150^\circ + \alpha)$

Region 3 : $(270^\circ - \alpha) \le \omega t \le (270^\circ + \alpha)$

Region I $\quad (30-\alpha) \le \omega t \le (30+\alpha)$

In this region thyristor 5 and 4 conduct. Under this conduction pattern the converter circuit of Fig. 2.1 can be simplified to that shown in Fig 2.6(a). From this the following circuit equation is evident.

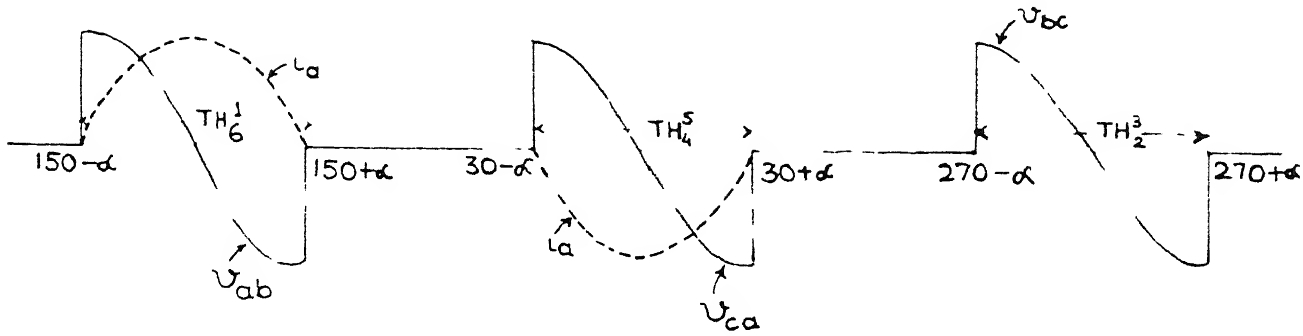

FIG 2.5 OUTPUT VOLTAGE AND INPUT CURRENT IN MODE -I

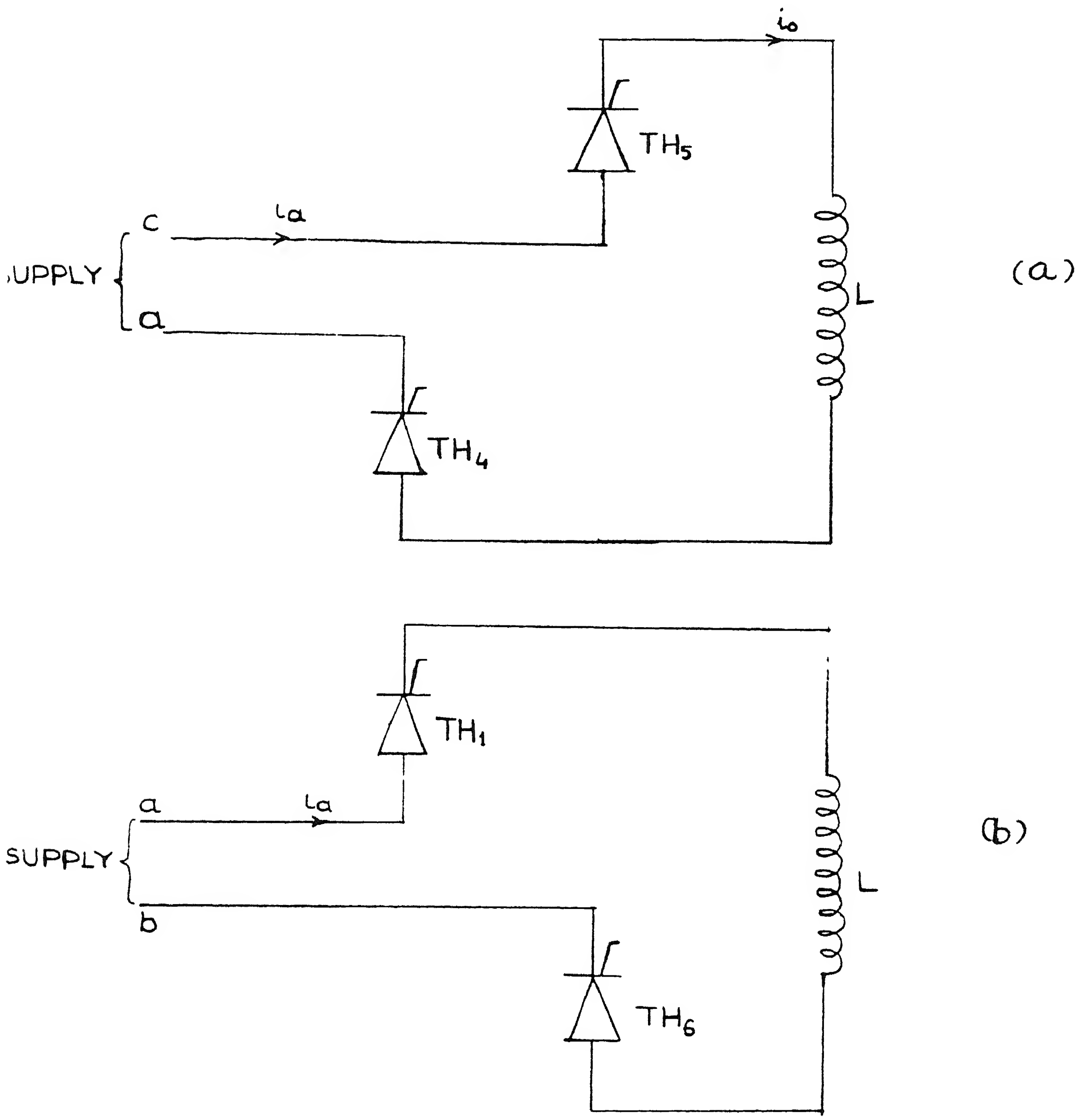

FIG 2 6 SIMPLIFIED CONVERTER CIRCUIT IN MODE -I

$$L\frac{di_o}{dt} = v_c - v_a = v_{ca} \qquad (2.4)$$

With $i_o = -i_a$, equation 2.4 is integrated to give

$$i_a = -\frac{\sqrt{3}\,V_m}{\omega L}\cos(\,\omega t + 150^\circ\,) + K_1 \qquad (2.5)$$

where K_1 is the constant of integration. This can be evaluated based on the boundary condition that at $\omega t = (30^\circ + \alpha)$, $i_a = 0$. Substituting the value of K_1, so obtained, the resulting expression for phase A current is

$$i_a = +\frac{\sqrt{3}\,V_m}{\omega L}\left[\cos(\omega t + 150) + \cos(\alpha)\right] \qquad (2.6)$$

Region II $(150-\alpha) \le \omega t \le (150+\alpha)$

In this region thyristors 1 and 6 conduct. The simplified converter circuit, in this case, is shown in Fig. 2.6(b), and the corresponding differential equation can be written as

$$L\frac{di_o}{dt} = v_{ab} \qquad (2.7)$$

with $i_o = i_a$, the above equation can be integrated and the integration constant can be evaluated using the boundary condition that at $\omega t = (150^\circ + \alpha)$, $i_a = 0$. The resulting expression for phase A current is

$$i_a = -\frac{\sqrt{3}\,V_m}{\omega L}\left[\cos(\omega t + 30) + \cos(\alpha)\right] \qquad (2.8)$$

Region III $(270^\circ - \alpha) \leq \omega t \leq (270^\circ + \alpha)$

In this case thyristors 3 and 2 conduct and hence the output is v_{bc}. Phase A current is zero in this case. The phase A input current waveform obtained using the derived equations (2.6) and (2.8) is shown in Fig. 2.7.

Fundamental component of phase A current

The fundamental component of phase A current can be expressed as

$$I_{a1} = c_1 \sin(\omega t + \phi_1) \qquad (2.9)$$

where

$$c_1 = \sqrt{a_1^2 + b_1^2} \qquad (2.10)$$

and

$$\phi_1 = \tan^{-1}\left(\frac{a_1}{b_1}\right) \qquad (2.11)$$

a_1 and b_1 are Fourier coefficients of fundamental component and evaluated as

$$a_1 = \frac{1}{2\pi}\left[\int_{30-\alpha}^{30+\alpha} i_a \cos(\omega t)\, d(\omega t) + \int_{150-\alpha}^{150+\alpha} i_a \cos(\omega t)\, d(\omega t)\right] \qquad (2.12)$$

$$b_1 = \frac{1}{2\pi}\left[\int_{30-\alpha}^{30+\alpha} i_a \sin(\omega t)\, d(\omega t) + \int_{150-\alpha}^{150+\alpha} i_a \sin(\omega t)\, d(\omega t)\right] \qquad (2.13)$$

Substituting i_a from (2.6) and (2.8) corresponding to appropriate intervals , a_1 and b_1 are obtained after subsequent integration and simplification, as

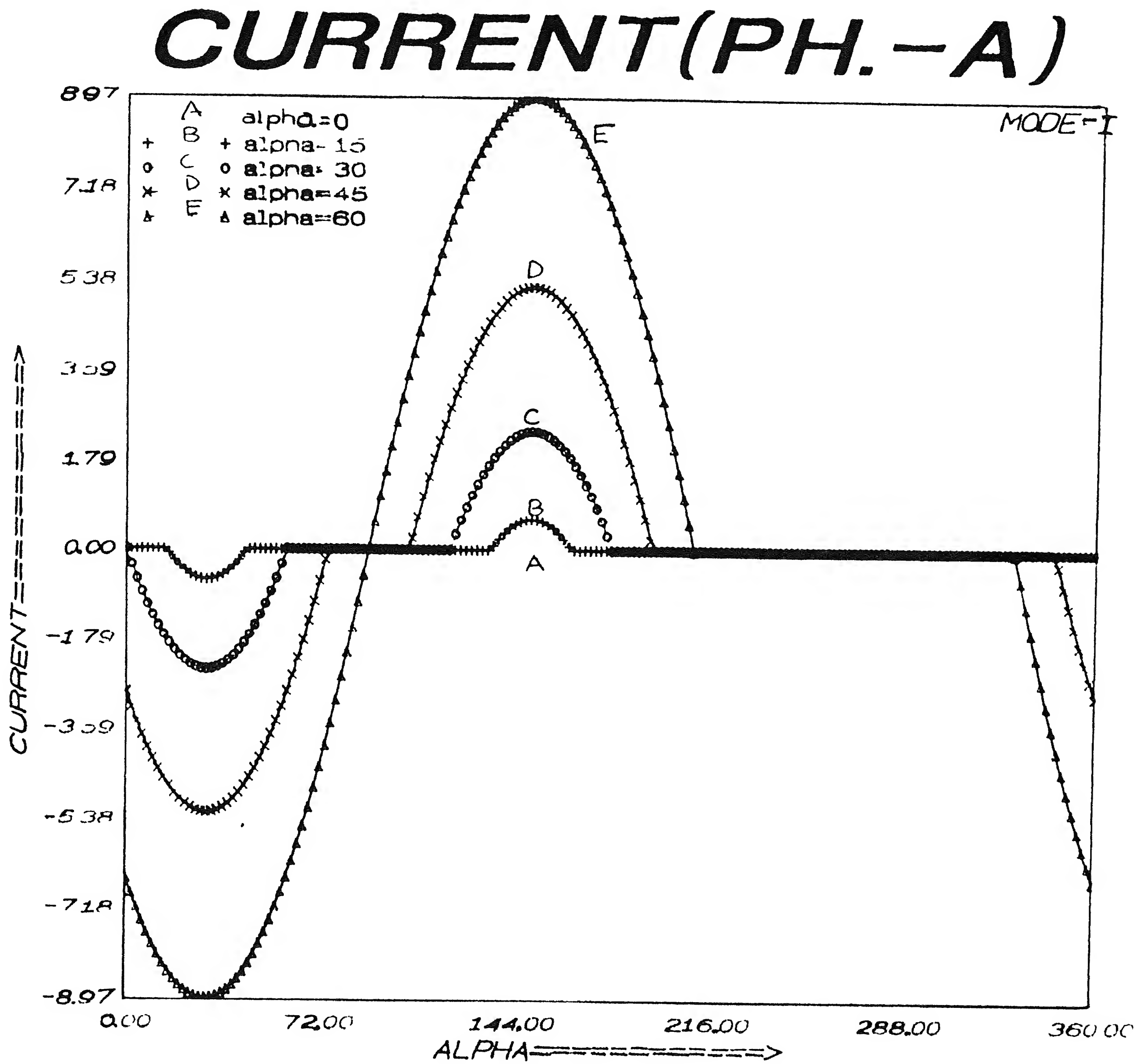

FIG 27 INPUT CURRENT OF PHASE -A (MODE -I)

$$a_1 = \frac{3\ V_m}{4\pi\omega L}\left[\sin\ (2\alpha) - (2\alpha)\right] \quad \text{and } b_1 = 0 \qquad (2.14)$$

Utilising equations (2.10) and (2.11), c_1 and ϕ_1 are evaluated as

$$c_1 = \frac{3\ V_m}{4\pi\omega L}\left[\sin\ (2\alpha) - (2\alpha)\right] \quad \text{and } \phi_1 = -90^\circ \qquad (2.15)$$

Substituting value of c_1 and ϕ_1 in equation (2.9) the fundamental component of phase A input current is obtained as

$$I_{a1} = \frac{3\ V_m}{4\pi\omega L}\left[\sin\ (2\alpha) - (2\alpha)\right] \sin\ (\omega t - 90) \qquad (2.16)$$

From equation (2.16) it is evident that fundamental component of phase A input current lags the corresponding phase A voltage by 90°. It is expected since the TCR inductance has been assumed to be ideal.

Similarly, expressions for fundamental component of phase B and C input current can be easily derived. In general, the fundamental component of input current in any phase can be given by the equation

$$I_{m1} = \frac{3\ V_m}{4\pi\omega L}\left[\sin\ (2\alpha) - (2\alpha)\right] \sin\ (\omega t - 90 + m.120) \qquad (2.17)$$

where m = 0, −1, +1 for phases A,B and C respectively.

2.2.2 Input Current in Mode II Operation

The output voltage waveforms under mode II operation ($60^\circ \leq \alpha \leq 120^\circ$) are shown in Fig. 2.3. From this, it can be observed that as α increases from 60° to 120°, the duration for which v_{ca},

v_{ab} and v_{bc} appear at the output, reduces. At $\alpha = 120^{\circ}$ they vanish altogether. On the contrary, at $\alpha = 60^{\circ}$, the duration of voltage pulses corresponding to v_{cb}, v_{ac} and v_{ba} is zero while it is maximum at $\alpha = 120^{\circ}$. At $\alpha = 90^{\circ}$, all the six line to line voltages appear at the output for equal duration. In general, the output voltage and the phase A input current in mode II operation is as shown in Fig. 2.8.

When thyristors 4 and 5 conduct the converter circuit of Fig. 2.1 can be simplified as shown in Fig. 2.9. From this following equation follows

$$L \frac{di_o}{dt} = v_c - v_a = v_{ca} \tag{2.18}$$

With $i_o = -i_a$, equation (2.18) is integrated, and using the boundary condition (at $\omega t = \alpha - 90^{\circ}$, $i_a = 0$) the expression for phase A current can be written as

$$i_a = \frac{\sqrt{3}V_m}{\omega L} \left[\cos(\omega t+150) - \cos(\alpha+60)\right] \quad \text{for } (\alpha-90) \le \omega t \le (150-\alpha) \tag{2.19a}$$

Similarly for other intervals, the phase A input current expression can be written as

$$i_a = \frac{-\sqrt{3}V_m}{\omega L} \left[\cos(\omega t+30) - \cos(\alpha+60)\right] \quad \text{for } (30+\alpha) \le \omega t \le (270-\alpha) \tag{2.19b}$$

$$= \frac{\sqrt{3}V_m}{\omega L} \left[\cos(\omega t+150) - \cos(\alpha-60)\right] \quad \text{for } (270-\alpha) \le \omega t \le (150+\alpha) \tag{2.19c}$$

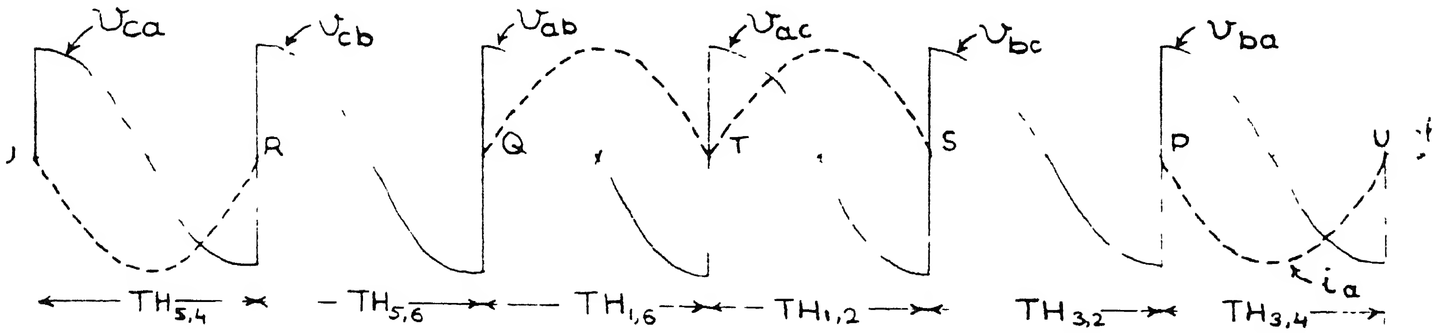

FIG 2.8 OUTPUT VOLTAGE AND INPUT CURRENT IN MODE -II

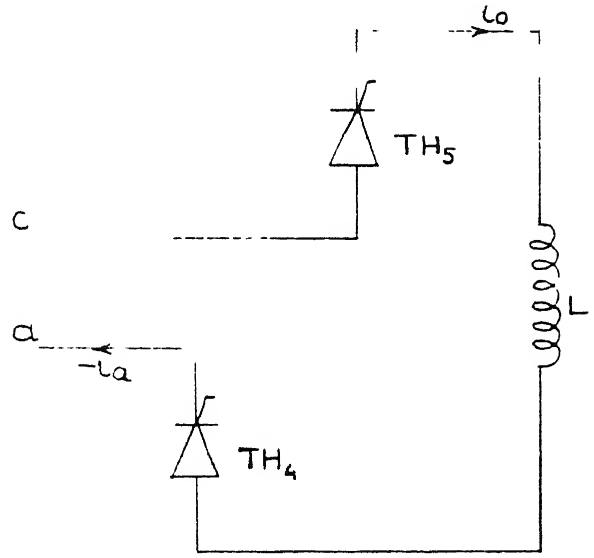

FIG 2.9 SIMPLIFIED CONVERTER CIRCUIT IN MODE -II

$$= -\frac{\sqrt{3}V_m}{\omega L}\left[\cos(\omega t+30) - \cos(\alpha-60)\right] \text{ for } (30-\alpha) \le \omega t \le (\alpha-90) \tag{2.19d}$$

$$= 0 \text{ otherwise}$$

The phase A input current in mode II plotted using equation (2.19(a) to 2.19(d)), is shown in Fig. 2.10.

Now, the fundamental component of phase A input current can be evaluated as in mode II operation. The Fourier coefficients of the fundamental component of phase A current in mode II can be written as

$$a_1 = \frac{1}{2\pi}\left[\int_{\alpha-90}^{150-\alpha} i_a \cos(\omega t)\, d(\omega t) + \int_{(\alpha+30)}^{-(\alpha+90)} i_a \cos(\omega t)\, d(\omega t)\right.$$

$$\left. + \int_{-(\alpha+90)}^{150+\alpha} i_a \cos(\omega t)\, d(\omega t) + \int_{30-\alpha}^{(\alpha-90)} i_a \cos(\omega t)\, d(\omega t)\right] \tag{2.20}$$

$$b_1 = \frac{1}{2\pi}\left[\int_{\alpha-90}^{150-\alpha} i_a \sin(\omega t)\, d(\omega t) + \int_{(\alpha+30)}^{-(\alpha+90)} i_a \sin(\omega t)\, d(\omega t)\right.$$

$$\left. + \int_{-(\alpha+90)}^{150+\alpha} i_a \sin(\omega t)\, d(\omega t) + \int_{30-\alpha}^{(\alpha-90)} i_a \sin(\omega t)\, d(\omega t)\right] \tag{2.21}$$

Utilising expressions for i_a from equations (2.19a) to (2.19d) appropriately, during different intervals, equation (2.20) and (2.21) will yield the following equation upon simplification

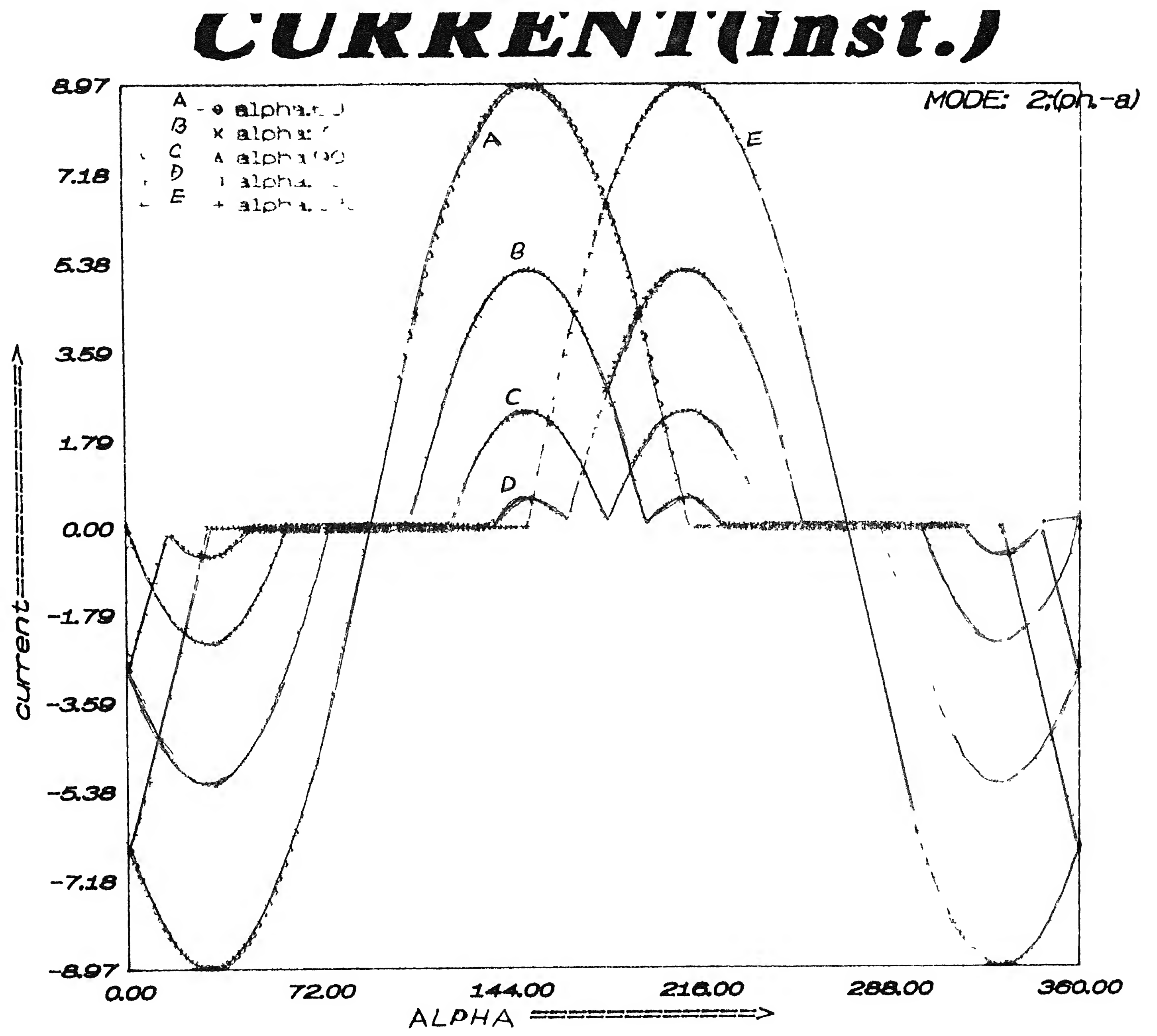

FIG 2.10 INPUT CURRENT OF PHASE -A (MODE -II)

$$a_1 = -\frac{\sqrt{3}\,V_m}{4\pi\omega L}\left[\frac{2\pi}{\sqrt{3}} + 3\cos(2\alpha)\right] \quad \text{and} \quad b_1 = 0 \tag{2.22}$$

c_1 and ϕ_1 can be obtained as

$$c_1 = |a_1| = \frac{\sqrt{3}\,V_m}{4\pi\omega L}\left[\frac{2\pi}{\sqrt{3}} + 3\cos(2\alpha)\right] \quad \text{and} \quad \phi_1 = -90^\circ \tag{2.23}$$

Substituting c_1 and ϕ_1 from equation (2.23) in equation (2.9) the fundamental component of phase A current as

$$I_{a1} = \frac{\sqrt{3}V_m}{4\pi\omega L}\left[\frac{2\pi}{\sqrt{3}} + 3\cos 2\alpha\right]\sin(\omega t - 90^\circ) \tag{2.24}$$

The fundamental component of phase B and C input current can be derived in similar manner. The generalized expression for fundamental component of phase current can be written as

$$I_{m1} = \frac{\sqrt{3}V_m}{4\pi\omega L}\left[\frac{2\pi}{\sqrt{3}} + 3\cos(2\alpha)\right]\sin(\omega t - 90 + 120m) \tag{2.24}$$

where m = 0,-1,+1 correspond to phase A,B and C respectively.

2.2.3 Input Current in Mode III Operation

The output voltage waveform in mode III is shown in Fig. 2.3. The output voltage comprises of voltage pulses corresponding to v_{cb}, v_{ac} and v_{ba}. It can be noted that the position of these output voltage pulses is displaced from that obtained in mode I 180°. The output voltage and mode III operation is, therefore, identical to that in mode I operation except that it is phase shifted by 180°. Consequently the phase A input current

expression for mode III operation can be obtained directly from mode I equations by using $180^\circ-\alpha$ in place of α. The phase A current waveform for various values of α is shown in Fig. 2.11.

2.3 TCR OPERATION WITH SOURCE INDUCTOR (L_s)

Unlike the convcentional converter operation, in the asymmetrical firing it is observed that there is no three valve conduction even when source inductance is taken into consideration. This can be illustrated considering $\alpha = 90^\circ$ whenvalves 4 and 5 (Fig. 2.1) are conducting at $\omega t = 0^\circ$ (refer Fig. 2.2). At $\omega t = 60^\circ$, valve 6 comes into conduction. Supposing valve 4 continue to conduct, voltage at cathode of valve 4 is $-v_c/2$ and at anode of valve 4, it is v_a. From Fig., 2.3 it can be seen that at $\omega t = 60^\circ$ $v_a > -v_c/2$ which indicates that the flow of current through valve 4 should reverse. Since this can not happen, valve 4 will turn off as soon as valve 6 is turn down. Thus, there is no period of three valve conduction.

Considering source inductance Fig. 2.12 shows a particular case of TCR operation with valves 4 and 5 conducting (region I of mode I as explained earlier). In this case the circuit equation can be written as

$$(2L_s + L)\ \frac{di_o}{dt} = v_{ca} \qquad (2.26)$$

with $i_o = -i_a$, integrating and using boundary condition same as equation (2.5), the input phase A current expression is obtained as

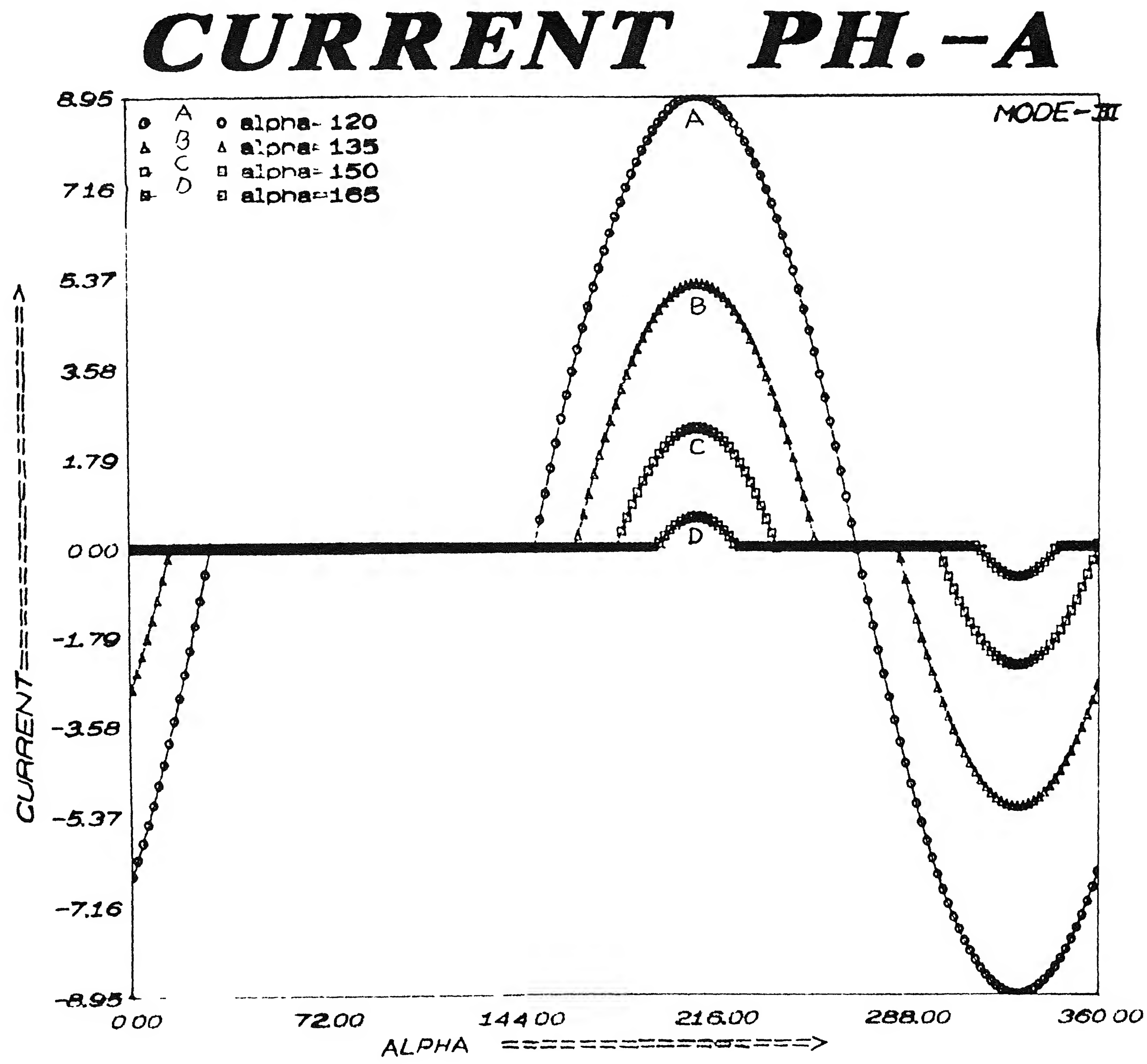

FIG 2.11 INPUT CURRENT OF PHASE -A (MODE -III)

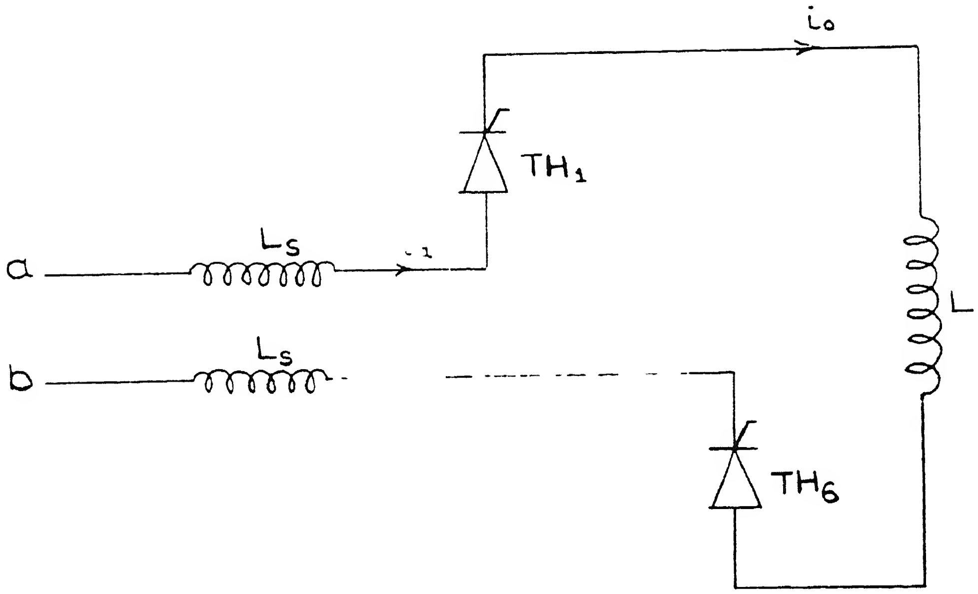

FIG 2.12 SIMPLIFIED CONVERTER CIRCUIT IN MODE -I (Ls CONSIDERED)

$$i_a = -\frac{\sqrt{3}\,V_m}{\omega(2L_s+L)}\left[\cos(\omega + 150) + \cos\alpha\right] \tag{2.27}$$

Equation (2.27) is similar to equation (2.6) except for the fact that L in equation (2.6) is replaced by $L_{eq} = 2L_s+L$ in equation (2.27). Therefore, the input phase current equations considering source inductance will be same as those obtained without source inductance except that L is replaced by L_{eq}. It is to be noted that effect of source inductance L_s is to reduce the peak value of phase current.

2.4 RMS INPUT CURRENT

The phase A input current in mode I operation is shown in Fig. 2.5. The rms input current expression is

$$I_{arms} = \frac{1}{2\pi}\left[\int_{30-\alpha}^{30+\alpha} (i_a)^2\, d(\omega t) + \int_{(150-\alpha)}^{150+\alpha} (i_a)^2\, d(\omega t)\right] \tag{2.28}$$

Utilising the phase A input current expressions (2.6) and (2.8), equation (2.28) yields on simplification

$$I_{arms1} = \sqrt{\frac{3}{2\pi}}\cdot\frac{V_m}{\omega L}\left[\sin(2\alpha) + 4\alpha\cos^2\alpha - 8\sin(\alpha) + 2\alpha\right]^{1/2} \tag{2.29}$$

In a similar manner the rms input current under mode II operation is obtained from Fig. 2.8 as

$$I_{arms2} = \sqrt{\frac{3}{2\pi}}\cdot\frac{V_m}{\omega L}\left[4(\frac{4\pi}{3} - \alpha) + (4 - \frac{4\pi}{3} - \sqrt{3})\sin 2\alpha + 2\sqrt{3}\alpha\sin(2\alpha)\right]^{1/2} \tag{2.30}$$

RMS rms input current expression for mode III operation can be obtained from equation (2.29) by substituting $(180^\circ-\alpha)$ in place of α.

2.5 OUTPUT RMS VOLTAGE

From Fig. 2.5 for mode I operation the output rms voltage expression can be written as

$$V_{orms1} = \left[\frac{1}{2\pi} \int_{30-\alpha}^{30+\alpha} v_{ca}^2 \, d(\omega t) + \int_{150-\alpha}^{150+\alpha} v_{ab}^2 \, d(\omega t) \right.$$

$$\left. + \int_{270-\alpha}^{270+\alpha} v_{bc}^2 \, d(\omega t) \right]^{1/2} \qquad (2.31)$$

Substituting the voltage equations (2.3), equation (2.31) can be simplified to

$$V_{orms1} = \frac{3V_m}{\sqrt{2\pi}} \left[\alpha - \sin(2\alpha) \right]^{1/2} \qquad (2.32)$$

Similarly from Fig. 2.8, of mode II operation the rms output voltage is obtained as

$$V_{orms2} = \frac{3V_m}{\sqrt{\pi}} \left[\alpha + \sin\,(120 + 2\alpha) + \sin\,(120-2\alpha) \right]^{1/2} \qquad (2.33)$$

The rms outpult voltage expression in mode III will be same as that of mode I given by equation (2.32), except that α is replaced by $180^\circ-\alpha$.

2 6 DISCUSSION

Asymmetrically triggered TCR has come up as a possible alternative to the conventional TCR A comparative evaluation of the two, however, should be made before the new scheme becomes practically viable.

The asymmetrical scheme makes use of only one inductor in place of three inductors in symmetrical scheme. In both the cases, the inductor is subjected to same maximum voltage ($\sqrt{2}$ V_{LL}) and hence no additional cost is incurred on the insulation The peak inverse voltage across the thyristor, in both the cases, is $\sqrt{2}$ V_{LL} i e. peak like to line voltage. The peak current through the thyristor in conventional TCR is ($\sqrt{2}$ $V_{LL}/\omega L$) while it is (0.31 $V_{LL}/\omega L$) (obtained from equation 2.16, at $\alpha = 60^{\circ}$) in case of asymmetrically triggered TCR in mode I. Therefore, with asymmetrically fired TCR, thyristors are economical. Thus from the device point of view, the asymmetrically triggered TCR conclusively, stands better. A further comparison, from harmonics and reactive power view point, should, however, be made.

2.7 CONCLUSION

In this chapter asymmetrically triggered TCR has been analysed in relation to input current, rms input current and rms output voltage The TCR operation, with source inductance taken into consideration, has been analysed. A comparative evaluation of symmetrically as well as asymmetrically triggered TCR from device point of view has been made.

Table 2.1 : Valve Conduction Pattern

<table>
<tr><th></th><th>0°</th><th colspan="2">60°</th><th colspan="2">120°</th><th colspan="2">180°</th><th colspan="2">240°</th><th colspan="2">300°</th><th>360°</th></tr>
<tr><td>$\alpha_p = 0°$</td><td>2,5</td><td>1,4</td><td colspan="2">1,4</td><td>1,4</td><td>3,6</td><td colspan="2">3,6</td><td>3,6</td><td>5,2</td><td colspan="2">5,2</td></tr>
<tr><td>$\alpha_p = 30°$</td><td colspan="2">5,4</td><td colspan="2">1,4</td><td colspan="2">1,6</td><td colspan="2">3,6</td><td colspan="2">3,2</td><td colspan="2">5,2</td></tr>
<tr><td>$\alpha_p = 60°$</td><td colspan="2">5,4</td><td>5,4</td><td>1,6</td><td colspan="2">1,6</td><td>1,6</td><td>3,2</td><td colspan="2">3,2</td><td>3,2</td><td>5,4</td></tr>
<tr><td>$\alpha_p = 90°$</td><td colspan="2">5,4</td><td>5,6</td><td>5,6</td><td colspan="2">1,6</td><td colspan="2">1,2</td><td colspan="2">3,2</td><td colspan="2">3,4</td></tr>
<tr><td>$\alpha_p = 120°$</td><td>3,4</td><td>5,6</td><td colspan="2">5,6</td><td>5,6</td><td>1,2</td><td colspan="2">1,2</td><td>1,2</td><td>3,4</td><td colspan="2">3,4</td></tr>
<tr><td>$\alpha_p = 150°$</td><td colspan="2">3,6</td><td colspan="2">5,6</td><td colspan="2">5,2</td><td colspan="2">1,2</td><td colspan="2">1,4</td><td colspan="2">3,4</td></tr>
<tr><td>$\alpha_p = 180°$</td><td colspan="2">3,6</td><td>3,6</td><td>5,2</td><td colspan="2">5,2</td><td>5,2</td><td>1,4</td><td colspan="2">1,4</td><td>1,4</td><td>3,6</td></tr>
</table>

CHAPTER - 3

HARMONIC ANALYSIS AND REACTIVE POWER GENERATION

The asymmetrically triggered thyristor controlled reactor is analysed further with regards to its reactive power generation capability and the harmonic content in various quantities like input current, output voltage and output current. This is an important aspect if the asymmetrically triggered TCR is to be used as an alternative to conventional TCR in Static VAR systems. In high power applications, injection of harmonics in the system are kept at the minimum if not totally avoided.

3.1 HARMONIC ANALYSIS

The harmonic components in input current, output voltage and current are calculated for all the three modes of TCR operation described in the previous chapter.

3.1.1 Harmonics in Input Current

The calculation of harmonic components is described below for phase A input current.

Mode I Operation

The phase A input current is shown in Fig. 2.5. Based on this, the general expression for the current can be written as

$$i_{an} = c_n \sin(n\omega t + \phi_n) \tag{3.1}$$

where
$$c_n = \sqrt{a_n^2 + b_n^2} \tag{3.2}$$

and
$$\phi_n = \tan^{-1}\left(\frac{a_n}{b_n}\right) \tag{33}$$

a_n and b_n denote the Fourier coefficients for n^{th} harmonic component. From Fig. 2.5 the expressions for these can be written as

$$a_n = \frac{1}{2\pi}\left[\int_{30-\alpha}^{30+\alpha} i_a \cos(n\omega t)\, d(\omega t) + \int_{150-\alpha}^{150+\alpha} i_a \cos(n\omega t)\, d(\omega t)\right] \tag{3.4}$$

$$b_n = \frac{1}{2\pi}\left[\int_{30-\alpha}^{30+\alpha} i_a \sin(n\omega t)\, d(\omega t) + \int_{150-\alpha}^{150+\alpha} i_a \sin(n\omega t)\, d(\omega t)\right] \tag{3.5}$$

where i_a is the input phase A current given by equations (2.6) and (2.8) which are reproduced below

$$i_a = \frac{\sqrt{3}\, V_m}{\omega L}\left[\cos(\omega t + 150^\circ) + \cos\alpha\right] \text{ for } (30^\circ - \alpha) \le \omega t \le (30^\circ + \alpha)$$

$$= \frac{-\sqrt{3}\, V_m}{\omega L}\left[\cos(\omega t + 30^\circ) + \cos\alpha\right] \text{for } (150^\circ - \alpha) \le \omega t \le (150^\circ + \alpha)$$

$$= 0 \text{ elsewhere}$$

Substituting i_a in equations (3.4) and (3.5), following expressions are obtained after integration and simplification

$$a_n = -\lambda_{n1} \sin(90n) \tag{3.6}$$

$$b_n = \lambda_{n1} \cos(90n) \tag{3.7}$$

where $$\lambda_{n1} = \frac{\sqrt{3}\, V_m}{\pi\, \omega\, L} \sin(60n) \left[\frac{\sin(\overline{n+1}\alpha)}{(n+1)} + \frac{\sin(\overline{n-1}\alpha)}{(n-1)} - \frac{2\cos(\alpha)\sin(n\alpha)}{n} \right] \tag{3.8}$$

and $n = 1,2,3 \ldots\ldots$.

As can be seen from Fig. 2.5, the dc component in the input current is zero and consequently

$$a_o = 0 \quad \text{and} \quad b_o = 0 \tag{3.9}$$

Utilising equations (3.6) to (3.8), the coefficient c_n and angle ϕ_n can be obtained as

$$c_n = |\lambda_{n1}| \tag{3.10}$$

and $$\phi_n = -90n \tag{3.11}$$

Substituting equations (3.10) and (3.11) in equation (3.1), gives

$$i_{an} = |\lambda_{n1}| \sin\{ n(\omega t - 90) \} \tag{3.12}$$

It is to be noted from equation (3.12) that all the triplen harmonics e.g. 3,6,9 ... etc. are zero. Utilising equation (3.10) the harmonic components present in the phase A input current can be calculated for various values of α. The variation of harmonic components with firing angle α is shown in Fig. 3.1. For these purpose, in Fig. 3.1, the phase A input current (i_{an}) is expressed as a ratio of fundamental component of phase A input current.

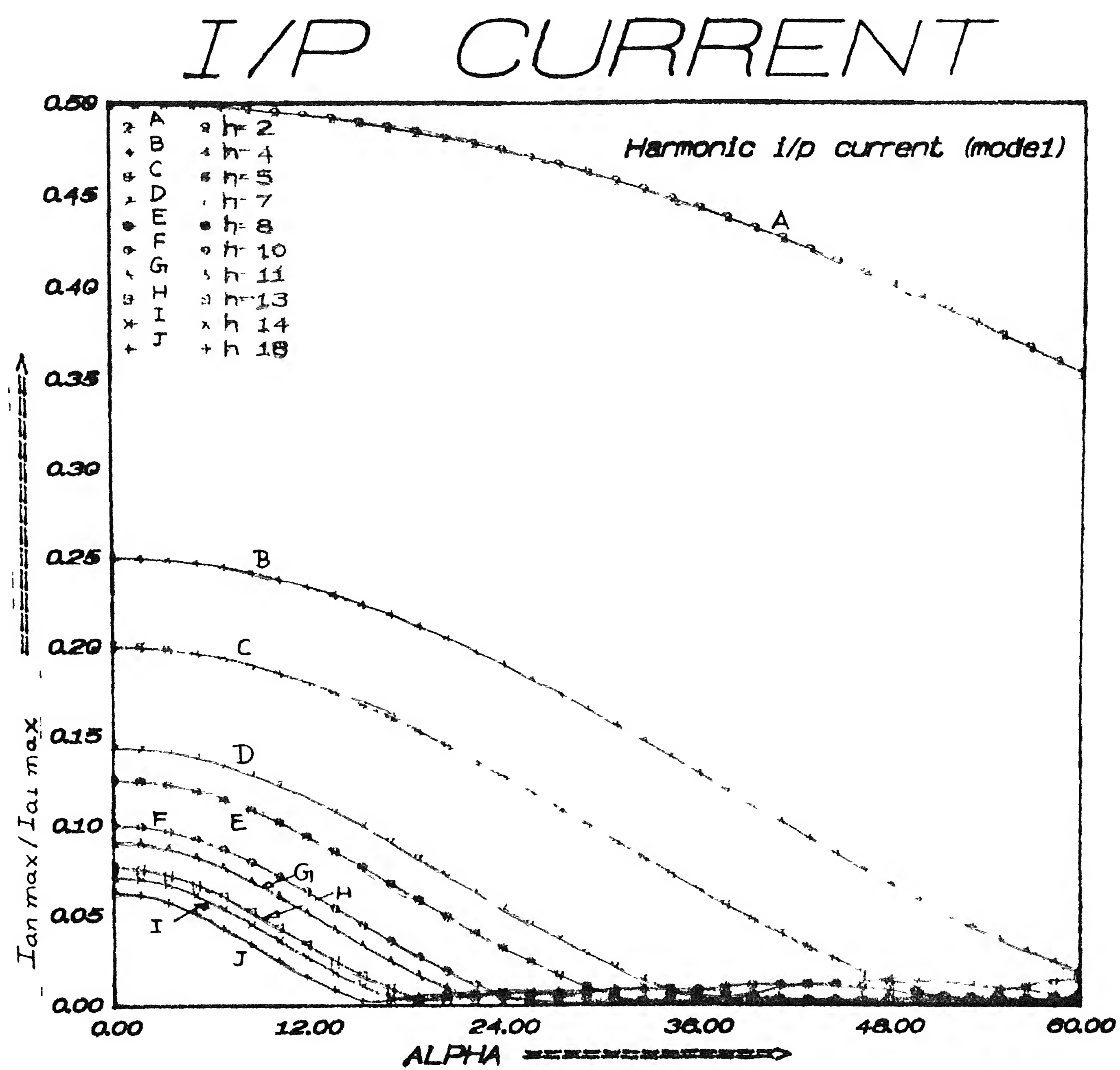

FIG. 3.1 HARMONIC COMPONENTS OF PHASE A INPUT CURRENT

The harmonic current expression for phases B and C in Mode I operation can be directly obtained from equation (3.12) by properly accounting for the 120° phase shift. In general, the expression for harmonic component of any phase can be writen as

$$I_n = |\lambda_{n1}| \sin \{ n(\omega t - 90^\circ) + m\, 120^\circ \} \tag{3.13}$$

where m = 0, −1 and +1 is for phase A, B and C respectively.

Mode II Operation

Under this mode of operation the Fourier coefficients a_n and b_n required to derive the equation for input phase current can be written based on Fig. 2.8 as

$$a_n = \frac{1}{2\pi} \left[\int_{\alpha-90}^{150-\alpha} i_a \cos(n\omega t)\, d(\omega t) + \int_{\alpha+30}^{-(\alpha+90)} i_a \cos(n\omega t)\, d(\omega t) \right.$$

$$\left. + \int_{-(\alpha+90)}^{(150+\alpha)} i_a \cos(n\omega t)\, d(\omega t) + \int_{30-\alpha}^{\alpha-90} i_a \cos(n\omega t)\, d(\omega t) \right] \tag{3.14}$$

$$b_n = \frac{1}{2\pi} \left[\int_{(\alpha-90)}^{150-\alpha} i_a \sin(n\omega t)\, d(\omega t) + \int_{(\alpha+30)}^{-(\alpha+90)} i_a \sin(n\omega t)\, d(\omega t) \right.$$

$$\left. + \int_{-(\alpha+90)}^{(150+\alpha)} i_a \sin(n\omega t)\, d(\omega t) + \int_{30-\alpha}^{\alpha-90} i_a \sin(n\omega t)\, d(\omega t) \right] \tag{3.15}$$

where i_a is the input phase current given by equations (2.19), (2.21), (2.23) and (2.25) for the corresponding time intervals.

After integrating and simplifying equations (3.14) and (3.15), the expressions for a_n and b_n are obtained as given below

$$a_n = \frac{\sqrt{3}\ V_m}{4\pi\omega L}\left[\frac{P_7}{n+1} + \frac{P_8}{n-1} - \frac{P_1}{n}\right] \tag{3.16a}$$

$$b_n = \frac{\sqrt{3}\ V_m}{4\pi\omega L}\left[\frac{P_9}{n+1} + \frac{P_{10}}{n-1} + \frac{P_2}{n}\right] \tag{3.16b}$$

Using a_n and b_n, the magnitude c_n and ϕ_n by equations (3.2) and (3.3) respectively, can be evaluated as

$$c_n = \frac{\sqrt{3}V_m}{4\pi\omega L}\left(\lambda_{n2}^2 + \lambda_{n3}^2\right)^{1/2} \text{and} \qquad \phi_n = \tan^{-1}\left(\frac{\lambda_{n2}}{\lambda_{n3}}\right)$$

where $\lambda_{n2} = \left\{\frac{P_7}{n+1} + \frac{P_8}{n-1} - \frac{P_1}{n}\right\}$ and $\lambda_{n3} = \left\{\frac{P_9}{n+1} + \frac{P_{10}}{n-1} + \frac{P_2}{n}\right\}$

P_1, P_2, P_7, P_8, P_9, and P_{10} are given in Appendix A.

The harmonic component of input current can, therefore be given by equation (3.1) as

$$i_{an} = \frac{\sqrt{3}\ V_m}{4\pi\omega L}\left(\lambda_{n2}^2 + \lambda_{n3}^2\right)^{1/2}\sin\left[n\omega t + \tan^{-1}\left(\frac{\lambda_{n2}}{\lambda_{n3}}\right)\right] \tag{3.16c}$$

Similarly the harmonic components for phases B and C can be evaluated. The harmonic components present in phase A input current is plotted for various values of α in Fig. 3.2.

Mode III Operation

It has been observed in Chapter 2 that mode III equation can be derived from mode I equation by simply substituting $(180^\circ - \alpha)$ in

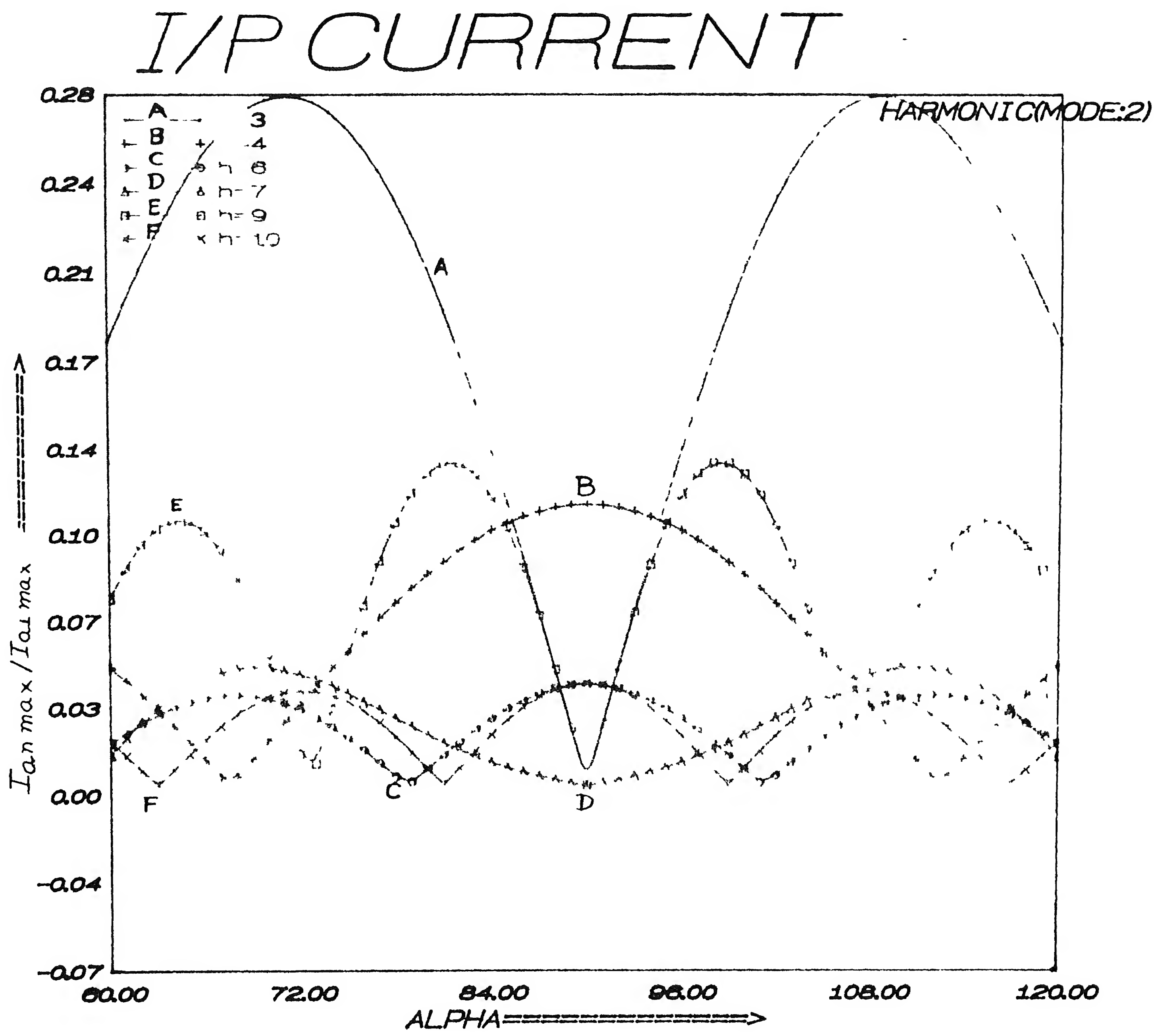

FIG 3 2 HARMONIC COMPONENTS OF PHASE A INPUT CURRENT

place of α and mode 3 are almost identical. Mode 3 equations can be obtained from corresponding mode 1 equations by using $(180-\alpha)$ in place of α. Based on this mode III equation here can be directly obtained as

$$i_{an} = |\lambda_{n4}| \sin(n\omega t - 90) \tag{3.17}$$

where

$$\lambda_{n4} = \frac{\sqrt{3}\, V_m}{\pi\omega L} \sin(60n) \left\{ \frac{\sin((n+1)(180^\circ-\alpha))}{(n+1)} + \frac{\sin((n-1)(180^\circ-\alpha))}{(n-1)} + \frac{2\cos\alpha\sin(n(180^\circ-\alpha))}{n} \right\}$$

The variation of harmonic components in input current with firing angle α is shown in Fig. 3.3.

3.1.2 Harmonics in Output Voltage

Mode I Operation

The output voltage (v_o) waveform is shown in Fig. 2.5. The output voltage (v_o) equals v_{ca} for $(30-\alpha) \leq \omega t \leq (30+\alpha)$, equals v_{ab} for $(150-\alpha) \leq \omega t \leq (150+\alpha)$, equals v_{bc} for $(270-\alpha) \leq \omega t \leq (270+\alpha)$. The Fourier coefficients of output voltage can be evaluated as

$$a_n = \frac{1}{2\pi} \int_0^{2\pi} v_o \cos(n\omega t)\, d(\omega t)$$

$$= \frac{1}{2\pi} \left[\int_{30-\alpha}^{30+\alpha} v_{ca} \cos(n\omega t)\, d(\omega t) + \int_{150-\alpha}^{150+\alpha} v_{ab} \cos(n\omega t)\, d(\omega t) \right.$$

$$\left. + \int_{270-\alpha}^{270+\alpha} v_{bc} \cos(n\omega t)\, d(\omega t) \right] \tag{3.18}$$

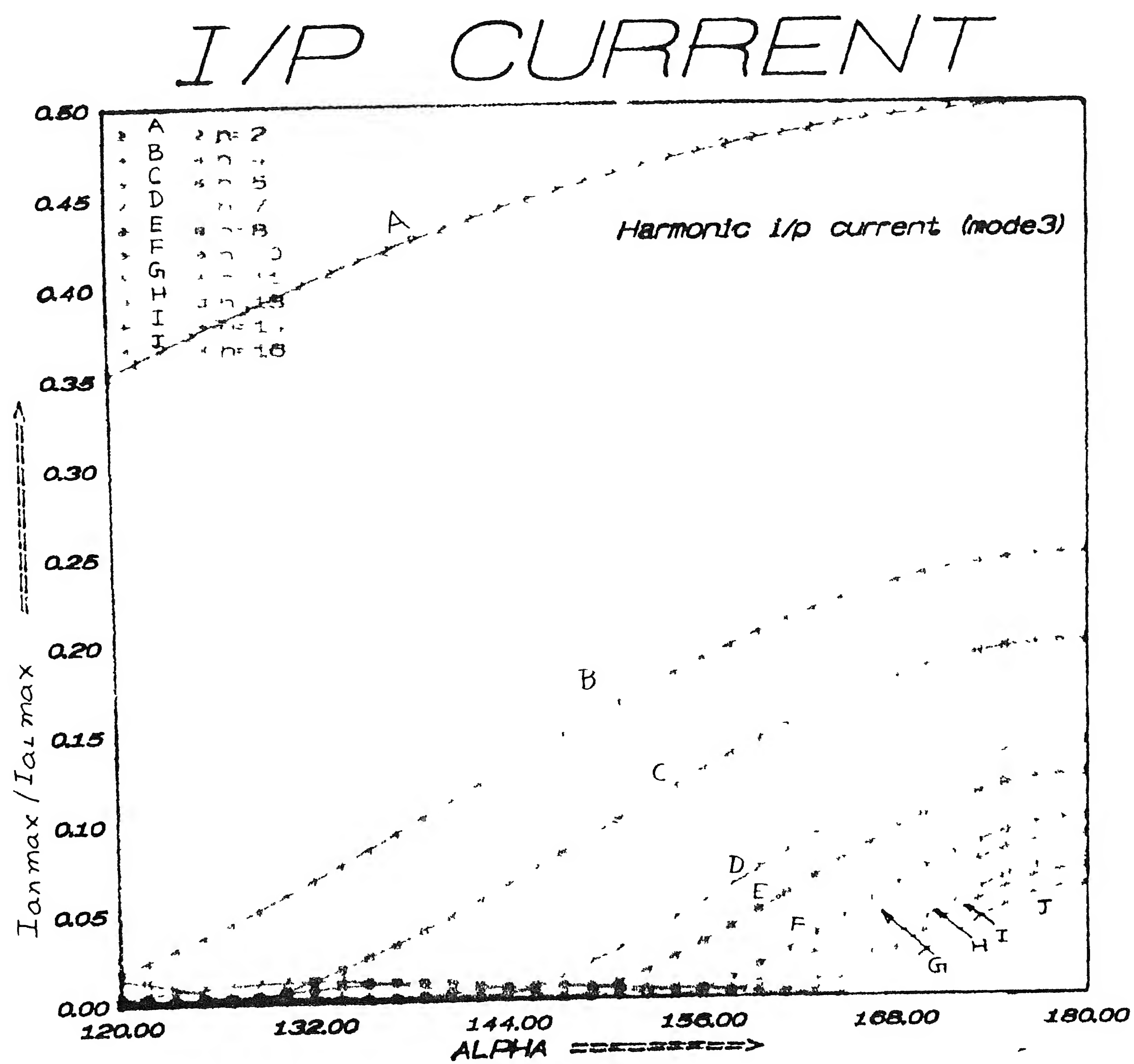

FIG 3 3 HARMONIC COMPONENTS OF PHASE A INPUT CURRENT

$$b_n = \frac{1}{2\pi}\int_0^{2\pi} v_o \sin(n\omega t)\, d(\omega t)$$

$$= \frac{1}{2\pi}\Bigg[\int_{30-\alpha}^{30+\alpha} v_{ca} \sin(n\omega t)\, d(\omega t) + \int_{150-\alpha}^{150+\alpha} v_{ab} \sin(n\omega t)\, d(\omega t)$$

$$+ \int_{270-\alpha}^{270+\alpha} v_{bc} \sin(n\omega t)\, d(\omega t)\Bigg] \tag{3.19}$$

Utilising equations (2.3a), (2.3b) and (2.3c), a_n and b_n can be obtained as

$$a_n = \beta_{n1} \sin(150n) \tag{3.20}$$

$$b_n = \beta_{n1} \cos(150n) \tag{3.21}$$

where $$\beta_{n1} = \frac{\sqrt{3}\, V_m}{2\pi} (1+\cos 120n)\left\{\frac{\sin((n+1)\alpha)}{(n+1)} - \frac{\sin((n-1)\alpha)}{(n-1)}\right\} \tag{3.22}$$

Therefore c_n and ϕ_n, defined by (3.2) and (3.3), can be written as

$$c_n = |\beta_{n1}| \quad \text{and} \quad \phi_n = (150n)$$

The harmonic components in output voltage can, therefore, be written as

$$v_{on} = |\beta_{n1}| \sin(n(\omega t + 150^\circ)) \tag{3.23}$$

From the equation (3.23), it is evident that there are no even harmonics in the output voltage.

Mode II Operation

The output voltage, in mode II operation, is shown in Fig. 2.8. From Fig. 2.8, using appropriate line to line voltage for the output, during different time intervals, the Fourier coefficients a_n and b_n can be evaluated as

$$a_n = \frac{\sqrt{3}\ V_m}{4\pi}\left[\frac{P_{11}}{n+1} + \frac{P_{12}}{n-1}\right] \tag{3.24a}$$

$$b_n = \frac{\sqrt{3}\ V_m}{4\pi}\left[\frac{P_{13}}{n+1} + \frac{P_{14}}{n-1}\right] \tag{3.24b}$$

where P_{11}, P_{12}, P_{13} and P_{14} are defined in Appendix A.

using a_n and b_n expression, the magnitude c_n and angle ϕ_n can be evaluated as

$$c_n = \frac{\sqrt{3}\ V_m}{4\pi}\left[\beta_{n2}^2 + \beta_{n3}^2\right]^{1/2} \text{ and } \phi_n = \tan^{-1}\left[\frac{\beta_{n2}}{\beta_{n3}}\right]$$

where $\beta_{n2} = \left[\frac{P_{11}}{n+1} + \frac{P_{12}}{n-1}\right]$ and $\beta_{n3} = \left[\frac{P_{13}}{n+1} + \frac{P_{14}}{n-1}\right]$

Substituting for the values of c_n and ϕ_n in equation (3.1), gives

$$v_{on} = \frac{\sqrt{3}\ V_m}{4\pi}\left[\beta_{n2}^2 + \beta_{n3}^2\right]^{1/2} \sin\left[n\omega t + \tan^{-1}\left(\frac{\beta_{n2}}{\beta_{n3}}\right)\right] \tag{3.24c}$$

Mode III Operation

Mode III output voltage equation can be derived from mode I equation by simply substituting $(180^\circ-\alpha)$ in place of α. Based on

this mode III output voltage equation can be directly obtained as

$$v_{on} = |\beta_{n4}| \quad \sin(n(\omega t+150^\circ)) \tag{3.25}$$

where

$$\beta_{n4} = \frac{\sqrt{3}\ V_m}{2\pi}\left[1+\cos(120n)\right]\left\{\frac{\sin((n+1)(180^\circ-\alpha))}{(n+1)} - \frac{\sin((n-1)(180^\circ-\alpha))}{(n-1)}\right\}$$

The variation of harmonic content in the output voltage is plotted as a function of α in Figs. 3.4 and 3.5 for mode I and mode III operation respectively. For this purpose, in Figs. 3.4 and 3.5 the harmonic content in the output voltage (v_{on}) is expressed as a ratio of maximum input phase to neutral voltage (v_m).

3.1.3 Harmonics in Output Current

Mode I operation

Based on the output current waveform shown in Fig. 3.6 the Fourier coefficients are obtained as

$$a_n = \frac{1}{2\pi}\left[\int_{30-\alpha}^{30+\alpha} i_c \cos(n\omega t)\ d(\omega t) + \int_{150-\alpha}^{150+\alpha} i_a \cos(n\omega t)\ d(\omega t) + \int_{270-\alpha}^{270+\alpha} i_b \cos(n\omega t)\ d(\omega t)\right] \tag{3.26}$$

$$b_n = \frac{1}{2\pi}\left[\int_{30-\alpha}^{30+\alpha} i_c \sin(n\omega t)\ d(\omega t) + \int_{150-\alpha}^{150+\alpha} i_a \sin(n\omega t)\ d(\omega t) + \int_{270-\alpha}^{270+\alpha} i_b \sin(n\omega t)\ d(\omega t)\right] \tag{3.27}$$

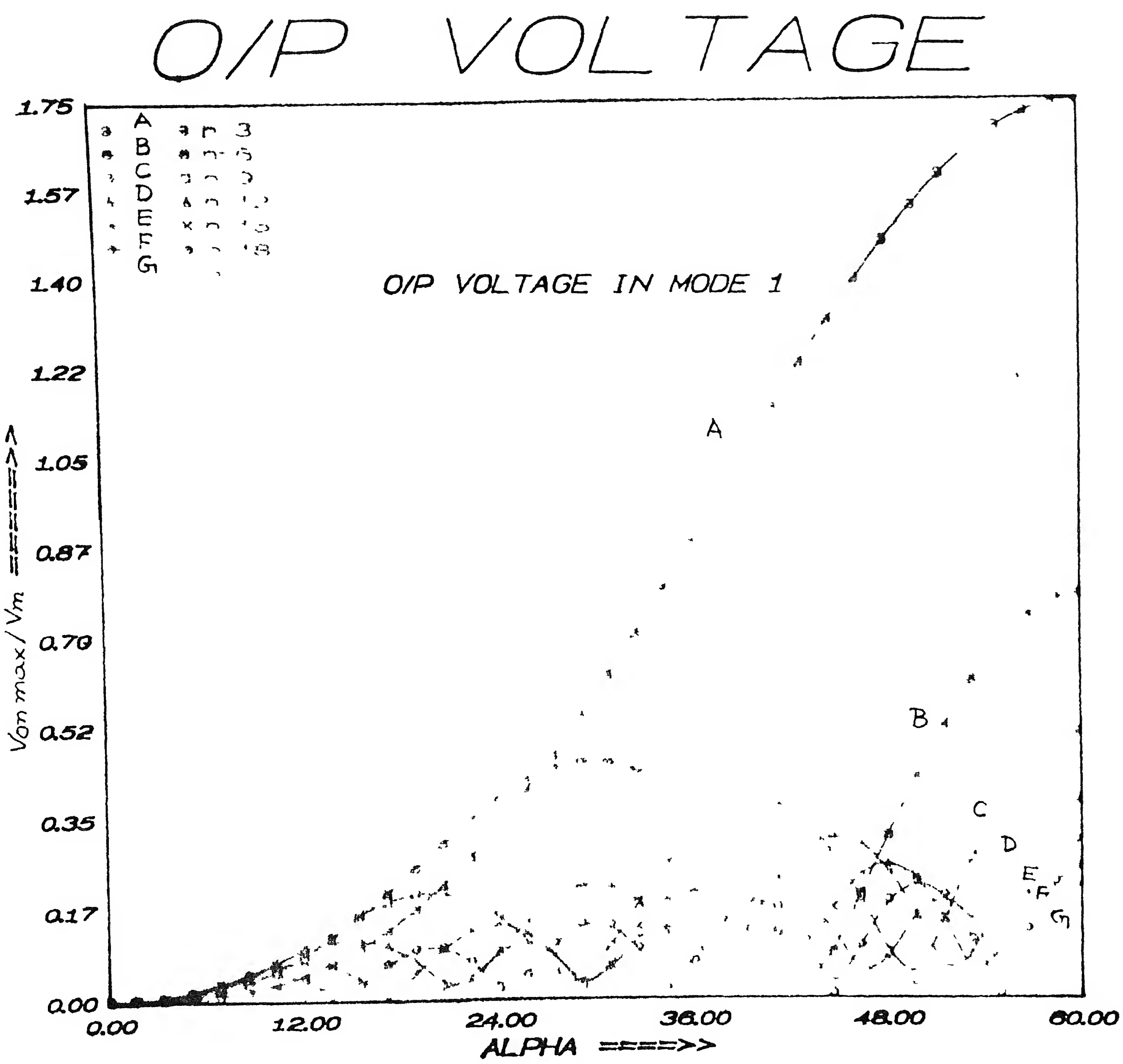

FIG 3 4 HARMONIC COMPONENTS OF OUTPUT VOLTAGE (MODE -I)

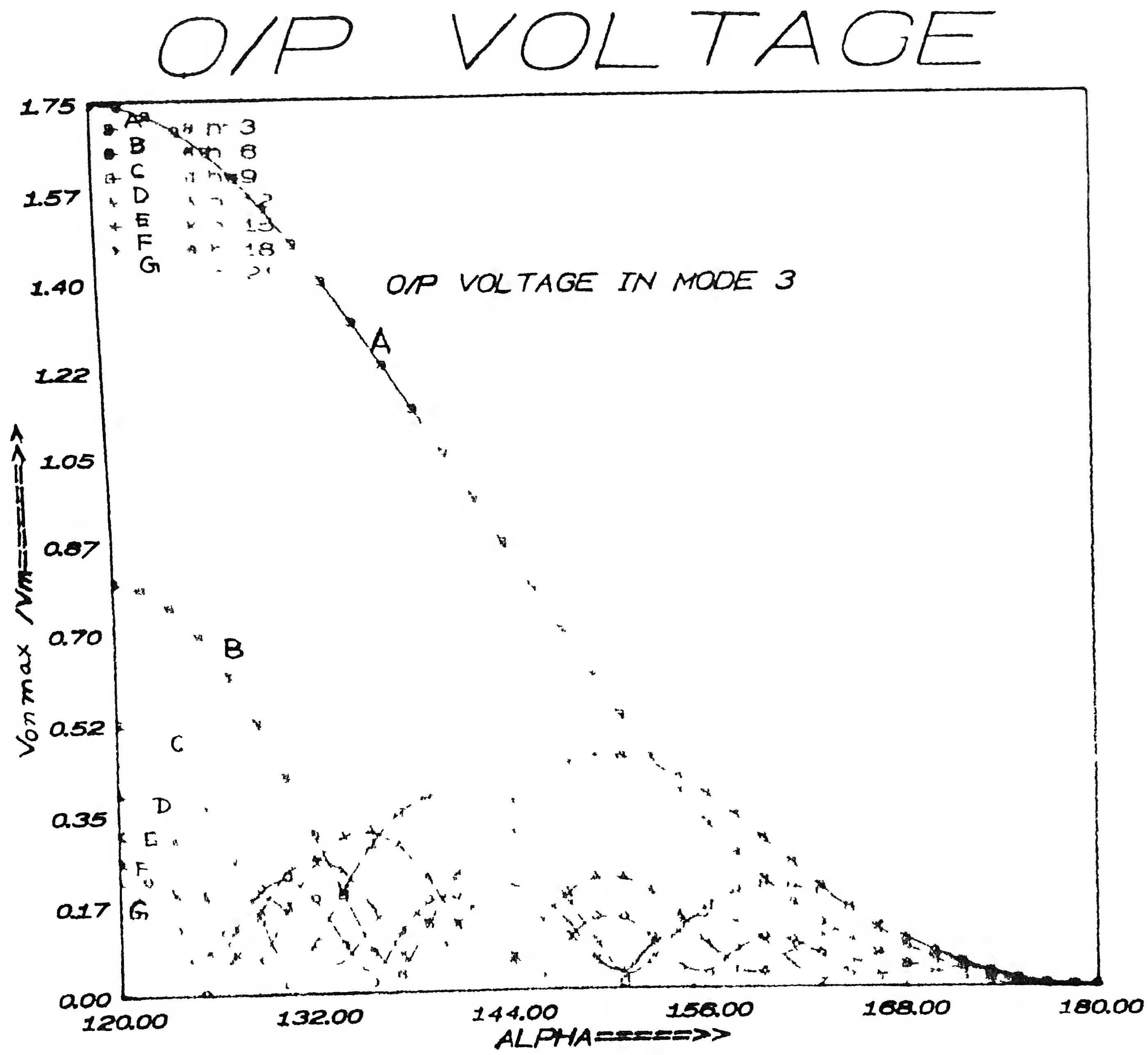

FIG 3 5 HARMONIC COMPONENTS OF OUTPUT VOLTAGE (MODE -III)

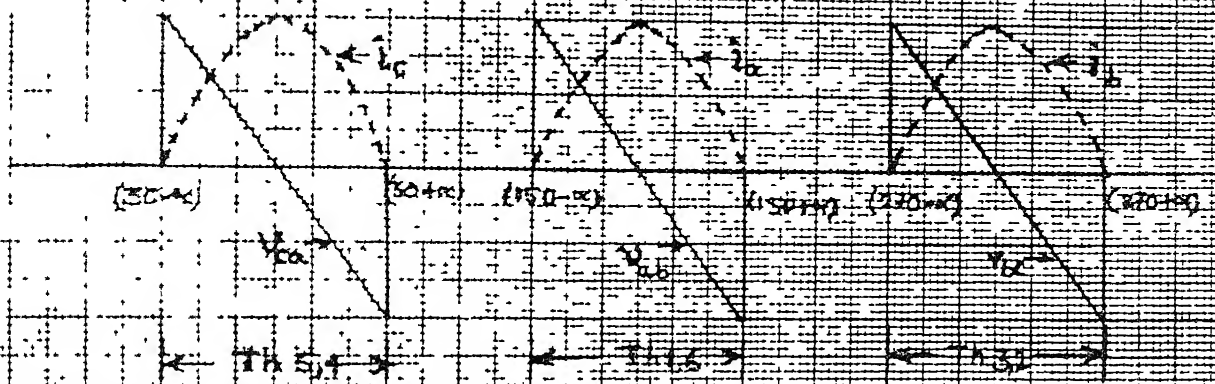

FIG 3 6 OUTPUT CURRENT WAVEFORM IN MODE -I

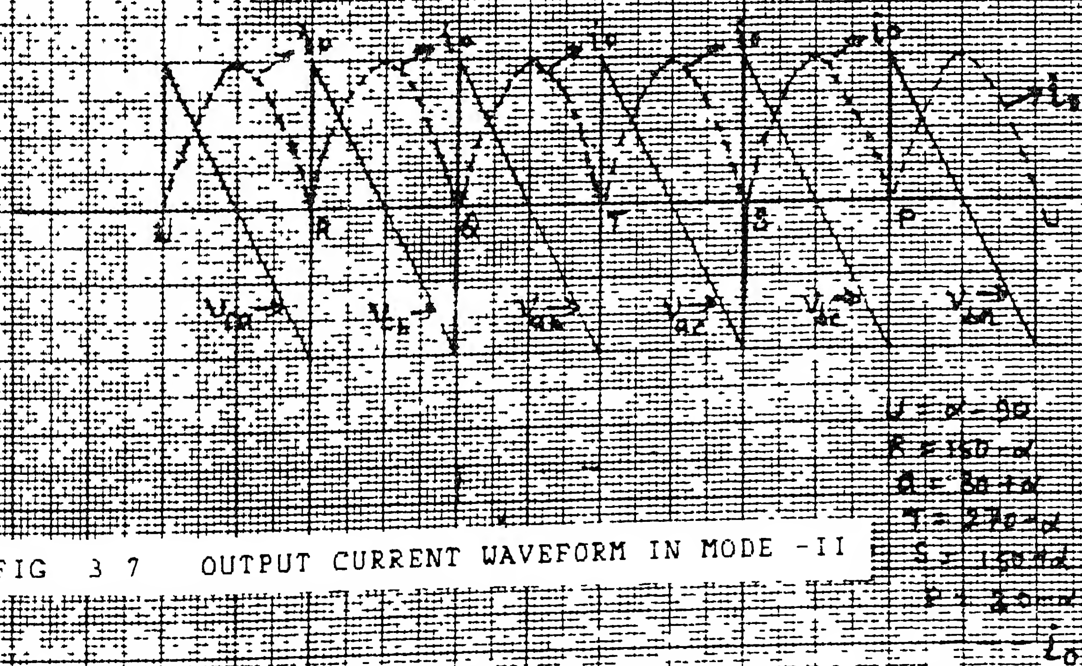

FIG 3 7 OUTPUT CURRENT WAVEFORM IN MODE -II

Equations (3.26) and (3.27) are written on the basis that during the interval $30-\alpha \le \omega t \le 30+\alpha$, i_a equals the output current. Similarly i_b and i_c equal the output current during interval $(150-\alpha) \le \omega t \le (150+\alpha)$ and $(270-\alpha) < \omega t \le (270+\alpha)$ respectively.

The input phase currents i_a, i_b and i_c valid under different time intervals are

$$i_a = -\frac{\sqrt{3}\ V_m}{\omega L}\left[\cos(\omega t + 30^\circ) + \cos(\alpha)\right] \text{for } (150^\circ-\alpha) \le \omega t \le (150^\circ+\alpha)$$

$$i_b = -\frac{\sqrt{3}\ V_m}{\omega L}\left[\cos(\omega t - 90^\circ) + \cos(\alpha)\right] \text{for } (270^\circ-\alpha) \le \omega t \le (270^\circ+\alpha)$$

$$i_c = \frac{-\sqrt{3}\ V_m}{\omega L}\left[\cos(\omega t + 150^\circ) + \cos(\alpha)\right] \text{for } (30^\circ-\alpha) \le \omega t \le (30^\circ+\alpha)$$

Substituting i_a, i_b and i_c in equations (3.26) and (3.27), the following expressions are obtained after simplification

$$a_n = \delta_{n1} \cos(150n) \tag{3.28}$$

$$b_n = \delta_{n1} \sin(150n) \tag{3.29}$$

where

$$\delta_{n1} = -\frac{\sqrt{3}\ V_m}{2\pi\omega L}\{1+2\cos(120n)\}\left\{\frac{2\cos(\alpha)\sin(n\alpha)}{n} - \frac{\sin(n+1)\alpha}{(n+1)} - \frac{\sin(n-1)\alpha}{(n-1)}\right\} \tag{3.30}$$

c_n and ϕ_n, defined earlier, are evaluated as

$$c_n = |\delta_{n1}| \quad \text{and} \quad \phi_n = -\frac{\pi}{2} + 150n$$

The resulting output current expression is

$$i_{on} = |\delta_{n1}| \sin(n(\omega t+150^\circ)-90^\circ) \tag{3.31}$$

From equation (3.31) it canbe observed that no harmonics other than triplen harmonics appear in the output current.

Model II Operation

From Fig. 3.7, it can be seen that during the interval $(\alpha-90) \le \omega t \le (150-\alpha)$ v_{ca} appears as the output voltage across inductor L. Under such a situation, the output current can be determined from

$$L \frac{di_o}{dt} = v_{ca}$$

Using expression for v_{ca} (equation (2.3c)) and integrating, the above equation with the boundary condition that at $\omega t = \alpha-90$, $i_o = 0$, the expression for output current is obtained as

$$i_o = - \frac{\sqrt{3}\, V_m}{\omega L} \left\{ \cos(\omega t + 150) - \cos(\alpha+60) \right\} \tag{3.32}$$

Similar expressions for the output current in the other time intervals, shown in Fig. 3.7 can also be derived. These are given below :

$$i_o = \frac{\sqrt{3}\, V_m}{\omega L} \left[\cos(\omega t - 90) - \cos(\alpha - 60) \right]; \quad (150-\alpha) \le \omega t \le (30+\alpha) \qquad .....(3.33)$$

$$= - \frac{\sqrt{3}\, V_m}{\omega L} \left[\cos(\omega t + 30) - \cos(\alpha + 60) \right]; \quad (30+\alpha) \le \omega t \le (270-\alpha) \qquad .....(3.34)$$

$$= + \frac{\sqrt{3}\, V_m}{\omega L} \left[\cos(\omega t + 150) - \cos(\alpha - 60) \right]; \quad (270-\alpha) \le \omega t \le (150+\alpha) \qquad .....(3.35)$$

$$= -\frac{\sqrt{3}\ V_m}{\omega L}\left[\cos\ (\omega t\ -\ 90) - \cos\ (\alpha + 60)\right];\ (150+\alpha)\le\omega t\le(30-\alpha)$$

.....(3.36)

$$= \frac{\sqrt{3}\ V_m}{\omega L}\left[\cos\ (\omega t\ +\ 30) - \cos\ (\alpha - 60)\right];\ (30-\alpha)\le\omega t\le(\alpha-90)$$

.....(3.37)

The Fourier coefficients a_n and b_n can be evaluated, in the usual manner, as

$$a_n = \frac{\sqrt{3}\ V_m}{4\pi\omega L}\left[\frac{P_{15}}{n+1} + \frac{P_{16}}{n-1} + P_3\cos(90n) + P_4\cos(150n) + P_5\right] \quad (3.38a)$$

$$b_n = \frac{\sqrt{3}\ V_m}{4\pi\omega L}\left[\frac{P_{17}}{n+1} + \frac{P_{18}}{n-1} + P_3\sin(90n) + P_4\sin(150n) + P_6\right] \quad (3.38b)$$

where P_3, P_4, P_5, P_6, P_{16}, P_{17} and P_{18} are defined in Appendix A. Utilising expression for a_n and b_n, the magnitude c_n and angle ϕ_n can be evaluated as given by equations (3.2) and (3.3). The resulting equation for the output current harmonic components is

$$i_{on} = \frac{\sqrt{3}\ V_m}{4\pi\omega L}\left[\delta_{n2}^2 + \delta_{n3}^2\right]^{1/2}\sin\left[n\omega t + \tan^{-1}\left(\frac{\delta_{n2}}{\delta_{n3}}\right)\right] \quad (3.38c)$$

where

$$\delta_{n2} = \left[\frac{P_{15}}{n+1} + \frac{P_{16}}{n-1} + P_3\cos(90n) + P_4\cos(150n) + P_5\right]$$

$$\delta_{n3} = \left[\frac{P_{17}}{n+1} + \frac{P_{18}}{n-1} + P_3\sin(90n) + P_4\sin(150n) + P_6\right]$$

Mode III Operation

The expression for harmonic components in output current in mode III operation can be directly obtained from equation (3.31) by substituting $(180^\circ-\alpha)$ in Place of α. The resulting expression for output current harmonic component is obtained as

$$i_{on} = |\delta_{n4}| \sin(n(\omega t+150^\circ) - 90^\circ) \tag{3.39}$$

where

$$\delta_{n4} = -\frac{\sqrt{3}\,V_m}{2\pi\omega L}\left[1+\cos(120n)\right]\left\{\frac{2\cos(180^\circ-\alpha)\sin(n(180^\circ-\alpha))}{n} - \frac{\sin(n+1(180^\circ-\alpha))}{(n+1)} - \frac{\sin(n-1(180^\circ-\alpha))}{(n-1)}\right\}$$

The variation of harmonic component in output current is plotted as a function of α in Figs. 3.8 and 3.9 for mode I and mode II operation respectively. For this purpose, in Figs. 3.8 and 3.9 the output current harmonic components (i_{on}) is expressed as a ratio of constant term K, defined in Figs. 3.8 and 3.9.

3.2 REACTIVE POWER ANALYSIS

Mode I Operation

The rms value of fundamental component of phase A input current is given by equation (2.6) as

$$I_{1rms} = \frac{3V_m}{4\sqrt{2}\,\pi\omega L}\,|\sin(2\alpha) - 2\alpha| \tag{3.40}$$

The reactive power drawn from phase A will be given by

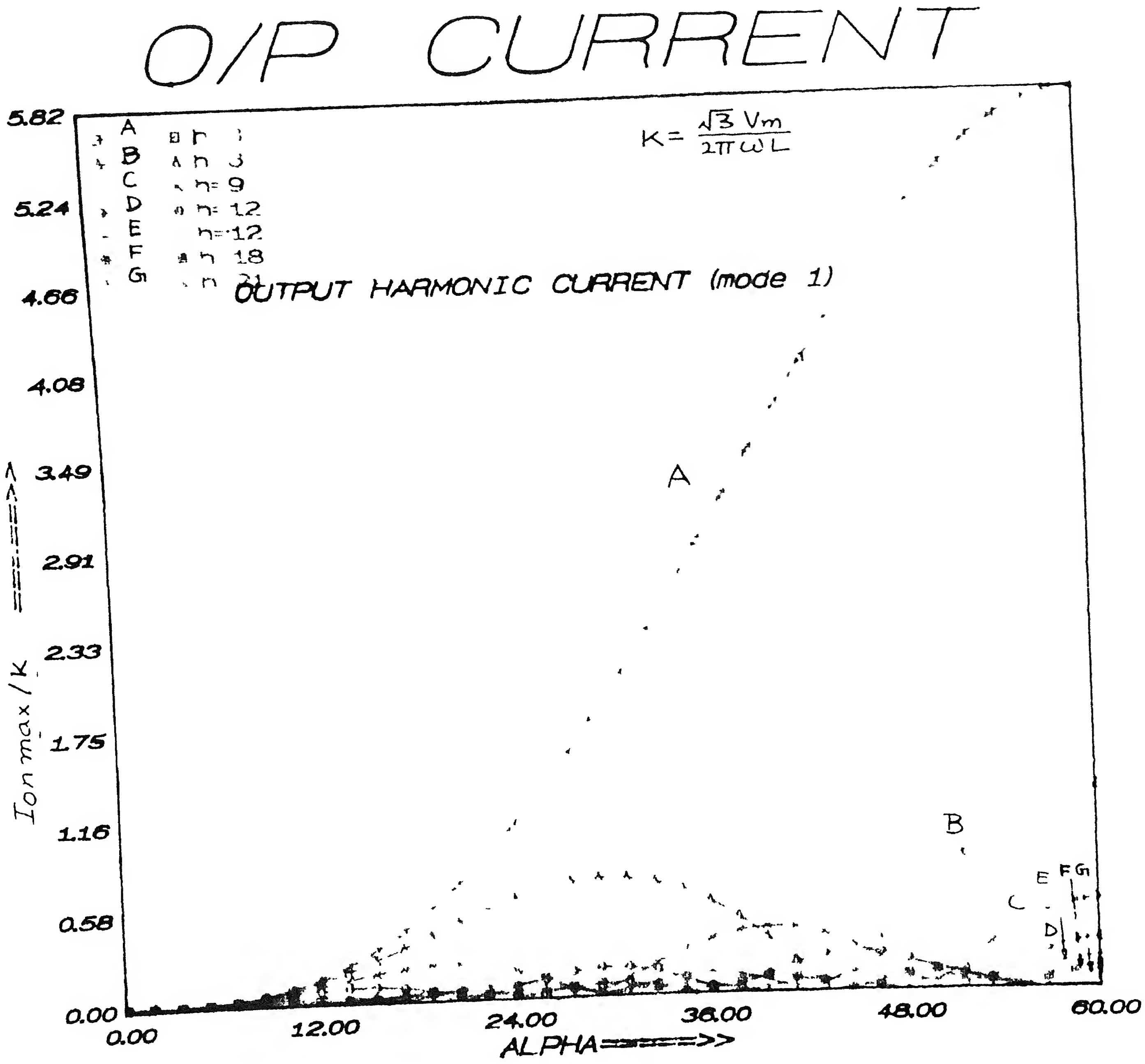

FIG 3 8 HARMONIC CONTENT IN OUTPUT CURRENT (MODE -I)

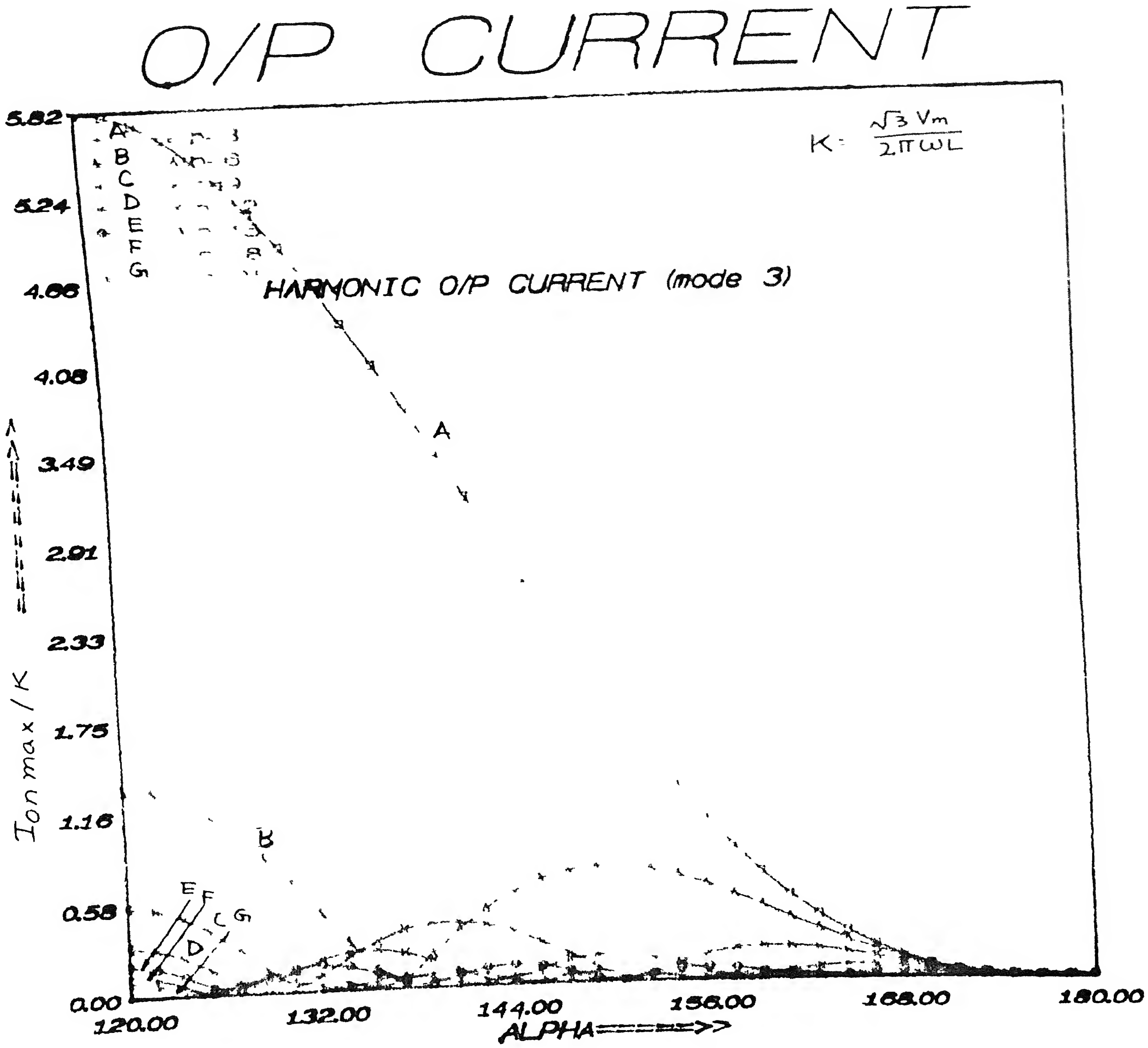

FIG 3 9 HARMONIC CONTENT IN OUTPUT CURRENT (MODE -III)

$$Q_A = V_{rms}\, I_{1rms} = \frac{3V_m^2}{8\pi\omega L}\left|\sin(2\alpha) - 2\alpha\right| \tag{3.41}$$

Therefore, the total reactive power from the source will be

$$Q_T = \frac{9V_m^2}{8\pi\omega L}\left|\sin(2\alpha) - 2\alpha\right| \tag{3.43}$$

Mode II Operation

The rms value of fundamental component of phase A input current is given by equation (2.30) as

$$I_{1rms} = \sqrt{\frac{3}{2}}\ \frac{V_m}{4\pi\omega L}\left(\frac{2\pi}{\sqrt{3}} + 3\cos(2\alpha)\right) \tag{3.44}$$

The reactive power drawn from phase A is given by

$$Q_A = \frac{\sqrt{3}\ V_m^2}{8\pi\omega L}\left(\frac{2\pi}{\sqrt{3}} + 3\cos(2\alpha)\right) \tag{3.45}$$

The total reactive power drawn from the source is given by

$$Q_T = \frac{3\sqrt{3}\ V_m^2}{8\pi\omega L}\left(\frac{2\pi}{\sqrt{3}} + 3\cos(2\alpha)\right) \tag{3.46}$$

Mode III Operation

The total reactive power drawn from the source, in mode III operation can be directly obtained from equation (3.43) by substituting $(180^\circ - \alpha)$ in place of α. The resulting equation is obtained as

$$Q_T = \frac{9V_m^2}{8\pi\omega L}\left|\sin(2(180^\circ - \alpha)) - 2(\pi - \alpha)\right| \tag{3.47}$$

To examine the reactive power generation capability the variation in reactive power is plotted with respect to the firing angle (α) for different modes of operation Equations (3 43), (3 46) and (3 47) have been used to obtain reactive power variation The results are plotted in Fig. 3.10. In the calculations of equations (3 43), (3.46) and (3.47) the peak value of input voltage (V_m) is chosen as $230\sqrt{2}$ volts and the value of inductor 'L' is taken as 100 mH with supply frequency of 50 Hz.

3.3 DISCUSSION

From the reactive power variation shown in Fig. 3.10, it is evident that while smooth control of reactive power over full range is possible under mode I and mode III operation, it is not quite so in mode II operation. Furthermore in mode II operation of the converter there are two values of firing angle corresponding to a particular reactive power requirement. Consequently a unique value of α for a particular value of reactive power requirement is not readily possible in mode II operation.

Based on the above observation, it appears better to consider the converter operation in either mode I or mode III. Since mode I and mode III operation are almost identical, the mode I operation can be considered as a practical choice. However, this must be evaluated with regards to harmonic content particularly in the input current since input current harmonics are injected into the supply system. The harmonic content in the input current

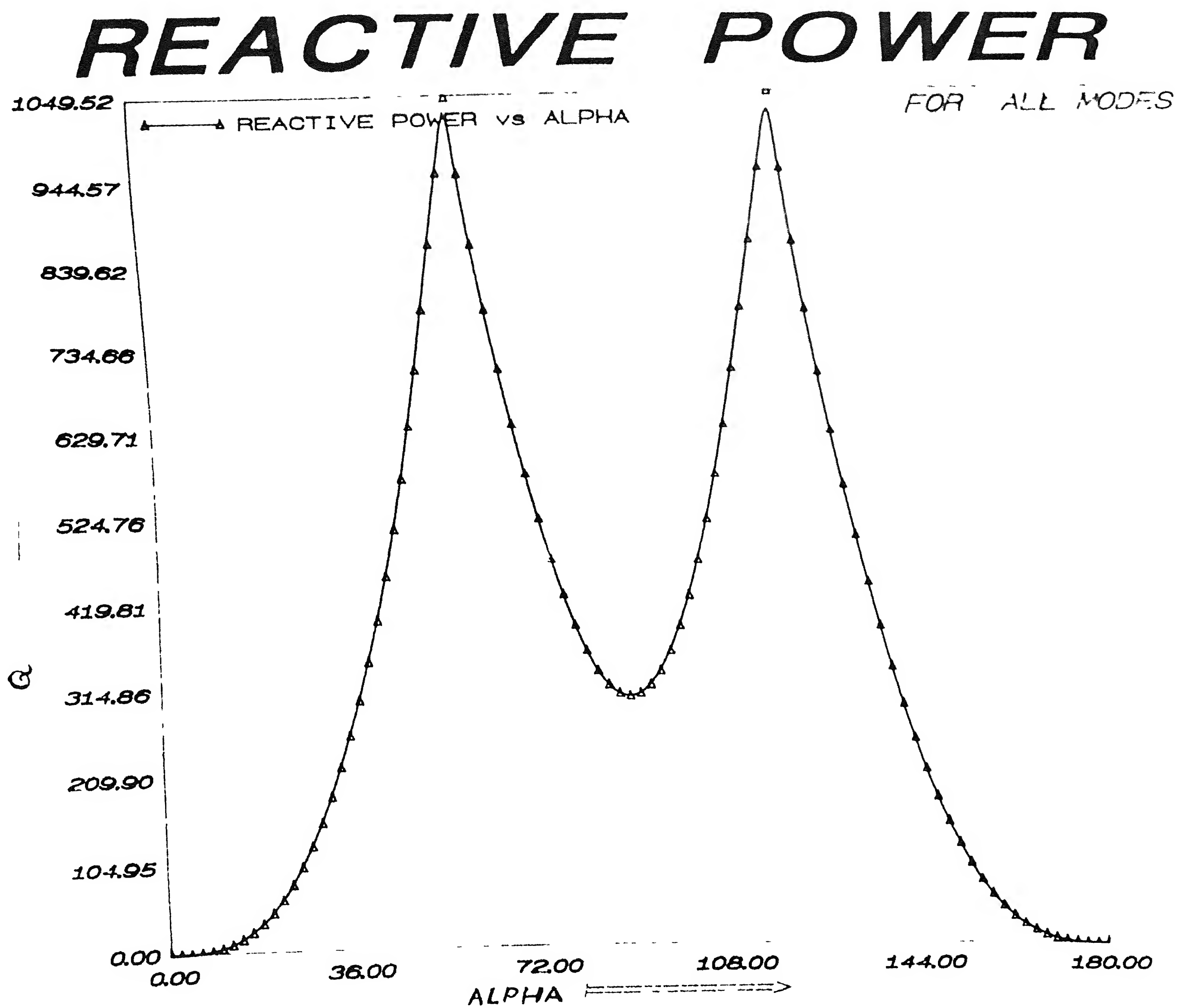

FIG 3 10 REACTIVE POWER VARIATION WITH ALPHA

under mode I operation is shown in Fig 3 1 It can be observed that in the lower range of firing angle harmonics of order less than 10 (2,4,5,7 and 8) are significant. Of these, the 2nd harmonic component is quite predominent However, if the firing angle is increased beyond 20°, all the harmonic components except 2,4 and 5 would reduce to less than 10% As a result the adverse impact of hiigher order harmonics may be substantially reduced.

As regards the other harmonics (2,4,5), separate filters may have to be provided for them. It may also be noticed from Fig. 3 10 that emposing a minimum firing angle limit of around 20° would not restrict the range of reactive power control appreciably

One important advantage is that the present scheme uses only one inductor On the output side of the converter, the inductor (L) is subjected to voltage having frequency components higher than the input voltage Because of this high frequency operation, the economic sizing of the inductor (L) is also possible.

As compared to the asymmetrically triggered TCR, the conventional TCR in SVS, has harmonics of the order of 6n±1 on the input side generally tuned filters are provided for 5th and 7th harmonics Asymmetrically triggered TCR would require one etra filter.

The maximum reactive power drawn by conventional TCR is given by $(3V_{LL}^2/\omega L)$ (V_{LL} line to line voltage) while it is $(0\ 3806V_{LL}^2/\omega L)$ [obtained from equation (3.43) at $\alpha = 60°$] in case

of asymmetrically fired TCR. Therefore, size of the inductor, for the same reactive power, in asymmetrically fired TCR is considerably small compared to the conventional TCR (L_{sym} = 7.88 L_{asym}).

Based on the above discussion, it is evident that certain measure as suggested, may be necessary to make asymmetrically triggered TCR practically viable as compared to the conventional TCR for Static VAR System application.

3.4 CONCLUSION

In this chapter asymmetrically triggered TCR has been analysed with regards to harmonic content in input current, output voltage output current, and its reactive power generation capability. It has been observed that unlike symmetrically triggered TCR which injects harmonics of the order 6n±1 into the supply system, asymmetrically triggered TCR injects even harmonics too. Based on the previous discussion, it has been concluded that restricting the minimum firing angle to about 20° has practical advantage from harmonics point of view, without appreciably reducing the controllable range of reactive power.

CHAPTER - 4

CASE STUDY

In previous chapters, the seady state performance of asymmetrically triggered TCR has been analysed It has been observed that this TCR, like conventional TCR which is symmetrically triggered, draws variable lagging reactive power from the source, and the reactive power drawn can be smoothly varied from zero to maximumum Therefore, it is expected that the asymmetrically triggered TCR can be used in place of conventional TCR in SVS for voltage control applications In this chapter, the study of sample system is undertaken to evaluate the efficacy of the asymmetrically triggered TCR with regard to its voltage control capability

4 1 THE STUDY SYSTEM

The system chosen for study is shown in Fig. 4.1. The system comprises of a generator feeding a 230 kV, 400 km long line On the other end of the line a variable load is connected. The asymmetrically triggered TCR alongwith fixed capacitor (FC) which together constitute a Static Var System is connected at the middle of the line to control the midpoint voltage as the load is varied The fixed capacitor includes the capacitive reactive power supplied by harmonic filter (2,4,5) at fundamental frequency. The systtem data is given in Appendix B. The size of

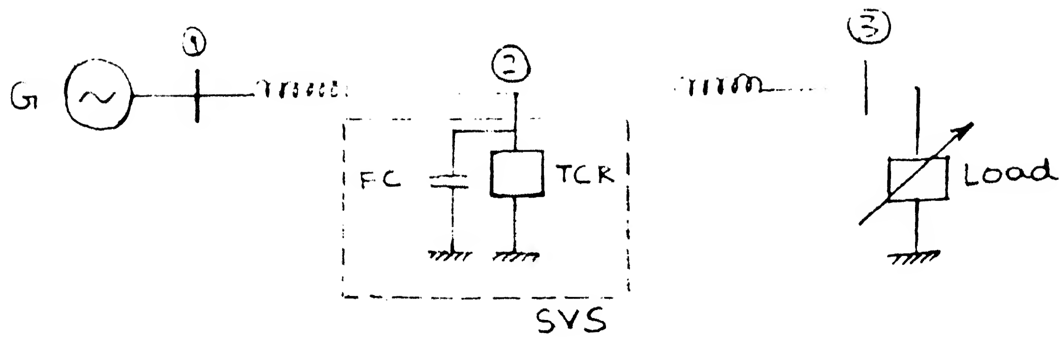

FIG 4.1 STUDY SYSTEM

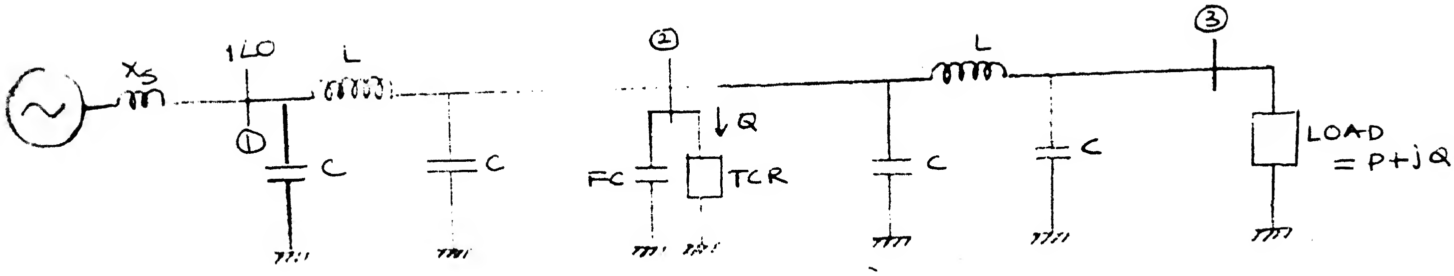

FIG 4.2 SYSTEM MODEL

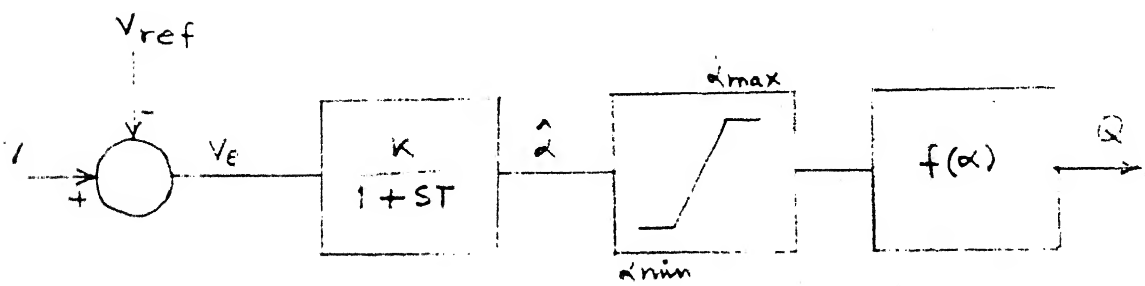

FIG 4.3 CONTROLLER BLOCK DIAGRAM

capacitor and inductor of TCR is determined based on load flow calculations as indicated below.

Constraints   Voltage at bus 1 = $1\angle 0$

Voltage at bus 2 = 0.98

The SVS bus is treated as PV bus, and load flow results for two extreme loading conditions are given below

S.No.	Load (MW, NVAR)	Bus 2 requirement injection) MVAR
1	0+j0	-220
2	500+j300	414

From the load flow result it is observed that at no load 220 MVAR should be drawn from bus 2, while at full load 414 MVAR reactive power should be injected into bus 2. The SVS should be designed to meet these reactive power requirements between the two extreme loading conditions. Based on the earlier discussion, the TCR operation is restricted to a minimum fring angle (α) of 20°

At full load the TCR operates at α_{min} Therefore, fixed capacitor should supply reactive power consumed by TCR at α_{min} in addition to the reactive power requirement at the bus 2 However, at no load, the TCR consumes the reactive power supplied by fixed capacitor in addition to the reactive power to be drawn from bus 2.

Based on above considerations,

Full capacity of TCR = 414 + 220 = 634 MVAR

Full capacity of TCR is reached at $\alpha = 60^{\circ}$ and hence it can be written that

$$Q_{TCR}\Big|_{\alpha=60^{\circ}} = \frac{9V^2}{4\pi\omega L_{TCR}}\Big[\sin(2\alpha) - (2\alpha)\Big]\Big|_{\alpha=60^{\circ}} = 634$$

For V = 230 kV , ω = 314 rad/sec, and L_{TCR} = 0 234 Henry.

$$Q \mid Q_{TCRmin} = Q_{TCR}\big|_{\alpha=60^{\circ}} = 28.6 \text{ MVAR}$$

Based on previous discussion,

Full capacity of capactor = 414 + 28 6 = 442.6 MVAR

Therefore fr V = 230 kV, C_{FC} = 26 64 μF.

4.2 SYSTEM MODEL

The complete system model is shown in Fig 4 2. The line on both sides of SVS is replaced by equivalent π network and the line resistance is neglected. The line transients are neglected and, hence, the line is described by algebraic equation , the generator is represented as an ideal volage source behind synchronous reactance (X_s). The TCR is assumed to operate in mode I, that is, $\alpha_{min} \leq \alpha \leq 60^{\circ}$, where α_{min} denotes the lower limit of firing angle which is taken here as 20° based on harmonic considerations. The reactive power observed by TCR, in model I, is given by following expression

$$Q = \frac{9V_m^2}{4\pi\omega L}\left[\sin(2\alpha) - (2\alpha)\right] = f(\alpha) \qquad (4\ 1)$$

4.3 CONTROL SCHEME

The firing angle control scheme is shown in Fig 4.3. V and V_{ref} are midpoint voltage (Fig. 4.2) and reference voltage respectively. The firing angle controller is basically a first order regulator which is fed with the voltage error v_c. The firing angle of TCR is adjusted depending upon the voltage error For a given firing angle, the reactive power is drawn by the TCR in accordance with equation (4.1).

The state equation for the firing angle controller is

$$\frac{d\hat{\alpha}}{d\tau} = -\frac{\hat{\alpha}}{T} + \frac{KV_e}{T} \qquad (4\ 2)$$

If $\hat{\alpha} \geq \alpha_{max}$, $\alpha = \alpha_{min}$ and if $\hat{\alpha} \leq \alpha_{min}$, α = α_{min}, otherwise $\alpha = \hat{\alpha}$

As discussed in the previous chapter, full range of reactive power variable is obtainable in mode I itself. Therefore α_{max} is chosen 60° so as to restrict the operation to mode I. Furthermore, as suggested in the previous chapter, α_{min} us kept at 20° in order to reduce the impact of harmonics.

4.4 RESULT

Two types of study have been performed on the system chosen

(a) System performance in response to variation in load

(b) System performance in response to variation in generator bus voltage

The system is initially supplying a reactive load of 150 MVAR The SVS bus voltage is maintained at 0.98 pu. Fig. 4.4(i) and 4.4(ii) show the effect of variation in load on SVS bus voltage and thyristor firing angle α respectively When the load is reduced to 25 MVAR at t = 0, the SVS bus voltage jumps up, but it is successfully brought down to about 0.98 pu through SVS control action. In this case thyristor firing angle, initially at 46°, goes up so that TCR draws more reactive power in order to bring down the SVS bus voltage. Conversely, when load is increased to 250 MVAR at t = 0, the SVS bus voltage goes down, but through the controller action, it is successfully maintained at about 0.98 pu. In this case, the thyristor firing angle is reduced so as to cut down the reactive power drawn by TCR. A load of 400 MVAR which is beyond the controllable range is also considered. In this case, it is observed that SVS is not able to maintain the SVS bus voltage at 0.98 pu even when thyristor firing angle hits its minimum Thus the fixed capacitor is not sufficient to provide the required amount of reactive power.

Fig 4 5(i) and 4.5(ii) shows the effect of variation in generator bus voltage on SVS bus voltage and thyristor firing angle (α) respectively. It is observed that when generator bus voltage is increased by 10% the SVS bus voltage also goes up, but it is successfully brought down to about 0.98 pu. The TCR firing

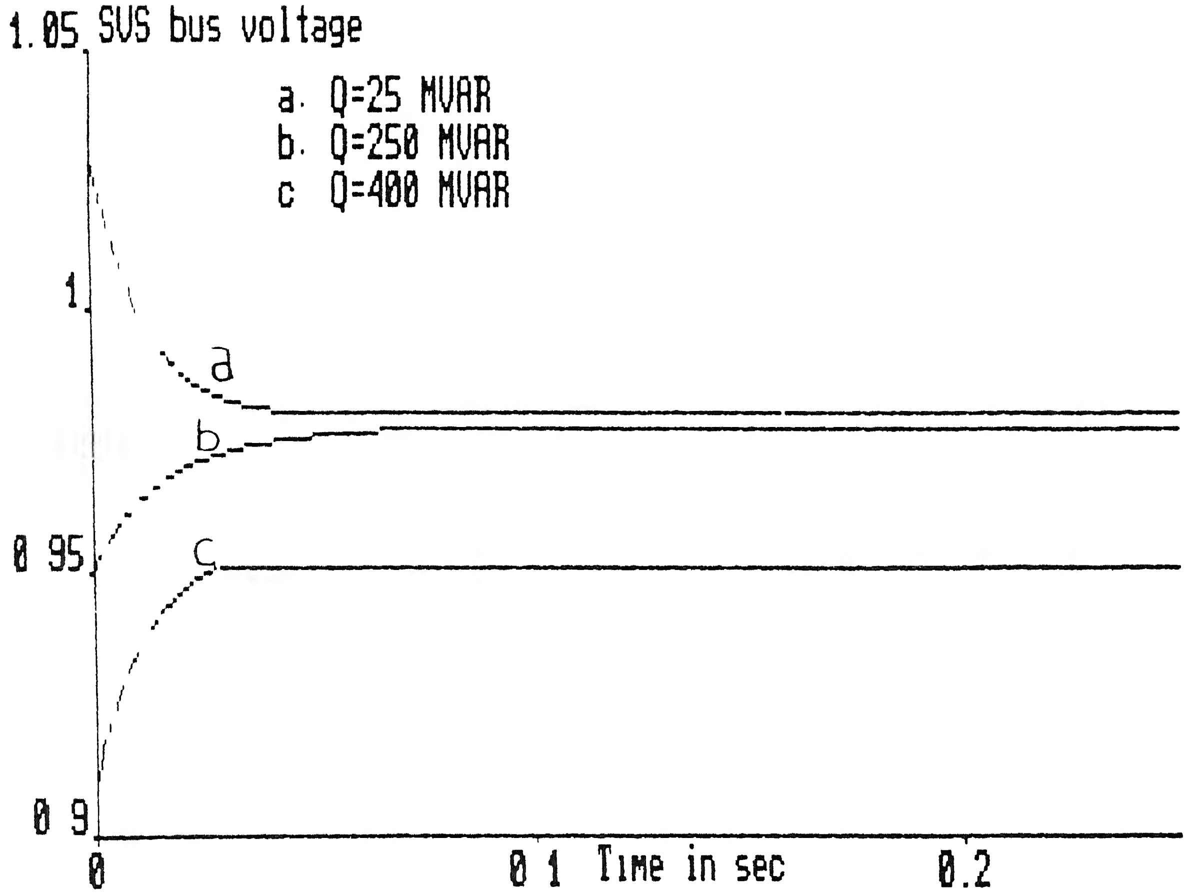
1.05 SVS bus voltage
a. Q=25 MVAR
b. Q=250 MVAR
c Q=400 MVAR
1
a
b
0 95
c
0 9
0
0 1 Time in sec
0.2

FIG 4 4(I)

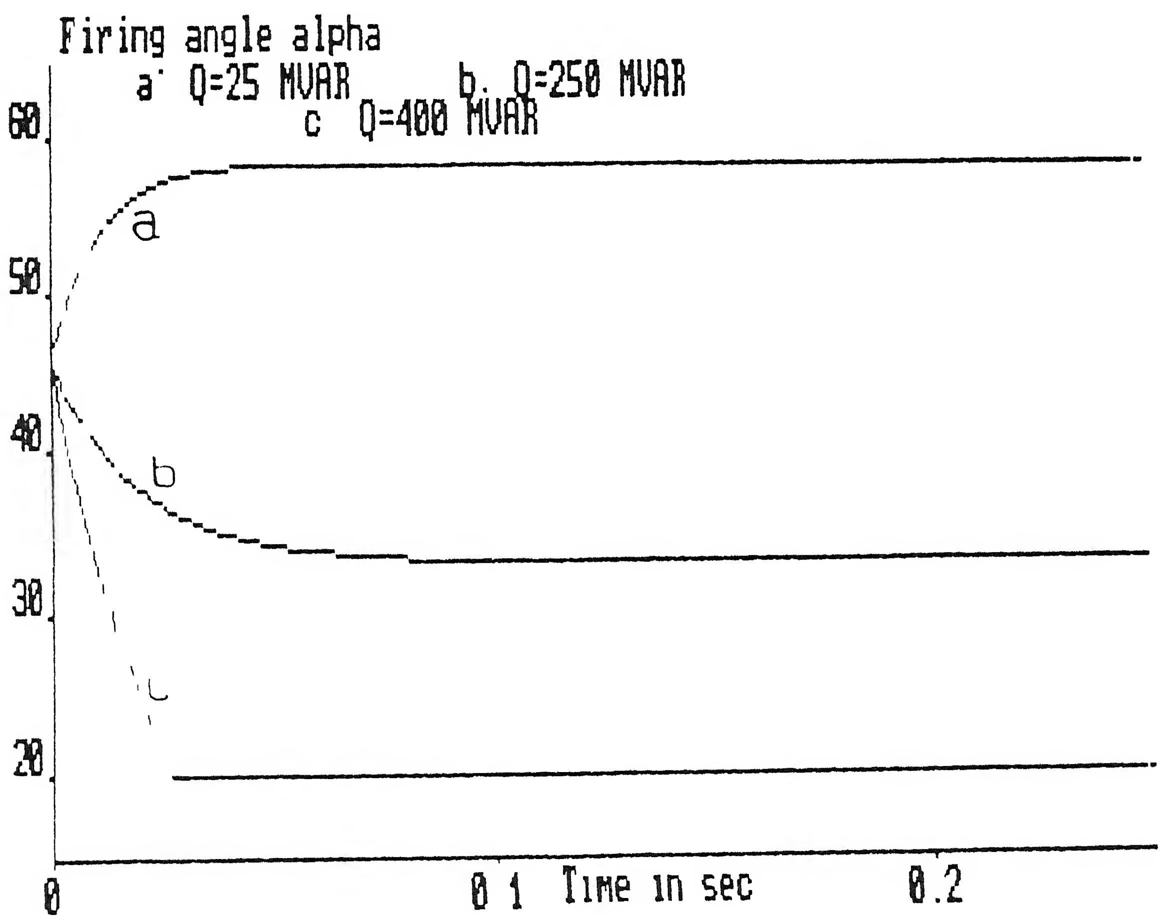
Firing angle alpha
a Q=25 MVAR
b. Q=250 MVAR
c Q=400 MVAR
60
a
50
40
b
30
c
20
0
0 1 Time in sec
0.2

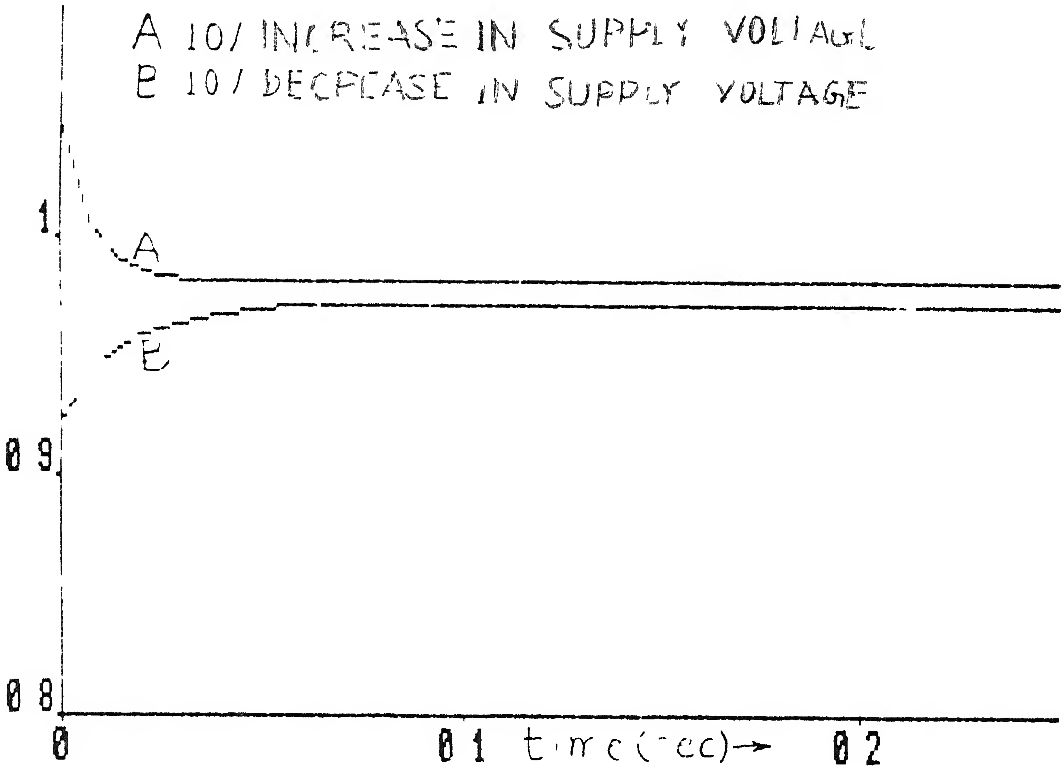

FIG 4 5(I)

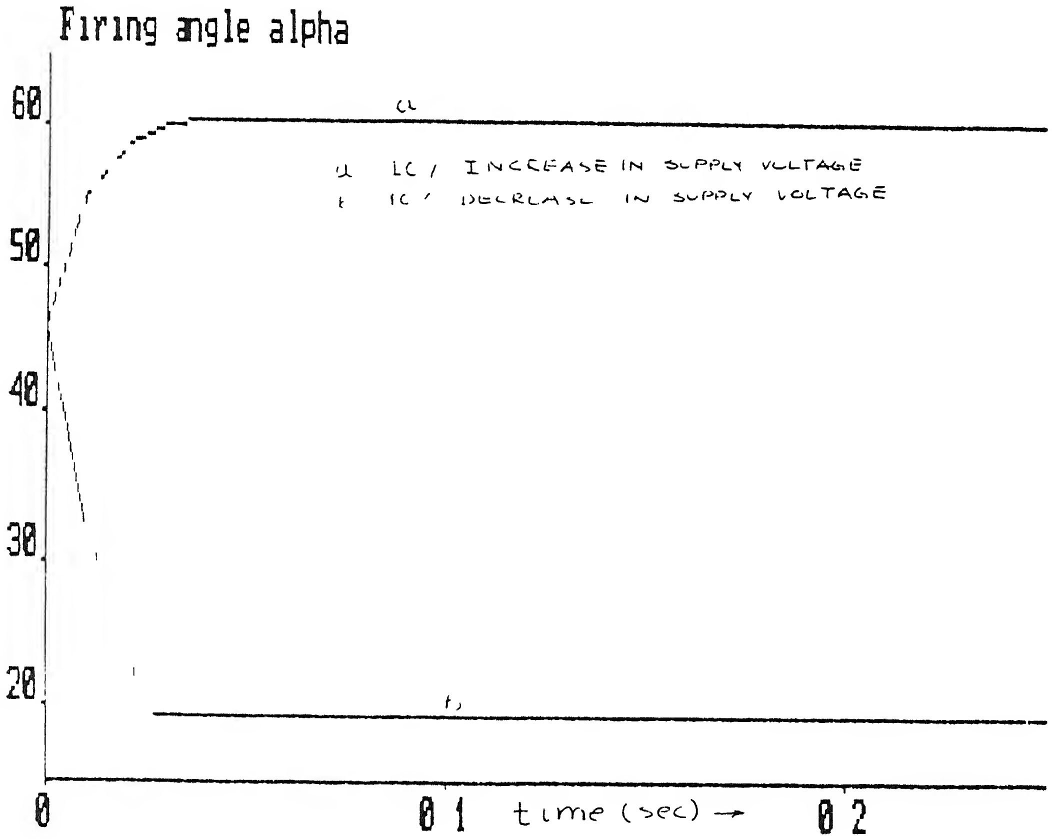

FIG 4 5(II)

FIG 4 5 EFFECT OF SUPPLY VOLTAGE VARIATION

angle hits its upper limit and the TCR draws maximum reactive power from the source in order to bring down the SVS bus voltage. Conversely, with 10% reduction in supply voltage, the thyristor firing angle hits its minimum, as a result the SVS supplies net capacitive reactive power to the system. The SVS is able to maintain the voltage at about 0 98 pu.

From the above discussion, it is obvious at least from the simplified analysis, that asymmetrically triggered TCR can be employed in place of conventional TCR in SVS application However, a more detailed transient analysis should be performed.

4 5 CONCLUSION

In this chapter a case study has been undertaken to assess the efficacy of asymmetrically triggered TCR in SVS applications. Two types of study have been performed in this regard It has been observed that utilisation of asymmetrically triggered TCR in place of conventional one gives expected result. However, a detailed transient studies on asymmetrically triggered TCR should be undertaken before it is successfully used in SVS applications

CHAPTER - 5

CONCLUSIONS

This thesis deals with the detailed investigation of the asymmetrically triggered TCR This TCR has been analysed with regards to input current, output voltage, reactive power generation capability and harmonic contents in various quantities, for all the three modes of operation A comparative evaluation of asymmetrical triggered TCR vis-a-vis conventional TCR has been made. A case study has been undertaken to assess the efficacy or otherwise of asymmetrically TCR in SVS applications.

The main conclusions that can be drawn from this thesis are :

(i) Compared to the conventional TCR, asymmetrically triggered TCR requires thyristor of smaller current rating. Furthermore, for the same reactive power, the size of inductor in asymmetrically triggered TCR is small.

(ii) Unlike the conventional TCR, in this new scheme of TCR no three valve conduction is observed when source inductance is taken into consideration However, the effect of source inductance is to reduce the peak of the phase current.

(iii) The smooth control of reactive power over full range is possible under mode I operation, but not in mode II operation Mode III operation being almost identical to mode I, the TCR operation can be restricted to mode I.

(iv) Asymmetrically triggered TCR, unlike conventional TCR, causes injection of even harmonics also into the supply system If a minimum firing angle limit of about 20° is imposed, all the harmonic components except 2,4 and 5 would reduce to less than 10% , without any reduction in the range of reactive power control

(v) It has been observed through simulation that asymmetrically triggered TCR can be successfully used in SVS applications

SCOPE OF FUTURE WORK

(i) A more detailed study of efficacy or otherwise of asymmetrically triggered TCR taking transients into consideration should be undertaken.

(ii) Selective elimination of harmonics through control modifications may be explored.

REFERENCES

[1] B.T. Byerly, D.T. Poznaniak and E R Taylor, Jr., "Static Reactive Compensation for Power Transmission Systems", ibid., Vol. PAS-101, pp. 3997-4005, Oct. 1982.

[2] T.J.E Miller, "Reactive Power Control in Electric Systems", John Wiley and Sons, New York, 1982.

[3] A. Olvegard, K. Walve, G Waglund, H. Frank and S. Torseng, "Improvement of Transmission Capacity by Thyristor Controlled Reactive Power", IEEE Trans. on PAS, Vol. PAS-100, pp. 3930-3939, Aug. 1981

[4] L. Gyugyi and E.R. Taylor, "Characteristics of Static, Thyristor Controlled Shunt Compensators for Power Transmission System Applications", IEEE Trans. on PAS, Vol. PAS-99, pp. 1795-1804, Sep./Oct. 1980.

[5] A.E. Hammad and R M. Mathur, "A New Generalized Concept for the Design of Thyristor Phase Controlled VAR Compensators Part I : Steady State Performance", IEEE Trans. on PAS, Vol PAS-98, pp 219-226, Jan /Feb. 1979

[5] A.E Hammad and R M Mathur, "A New Generalized Concept for the Design of Thyristor Phase Controlled VAR Compensators Part II · Transient Performance", IEEE Trans. on PAS, Vol. PAS-98, pp 227-231, Jan./Feb. 1979.

[7] L. Gyugyi, "Control of Shunt Compensation with Reference to New Design Concepts", IEE Proc Vol. 128, Pt.C, No. 6, pp 374-381, Nov 1981

[8] H. Boenig and E. Cibulka, "A Static VAR Compensator using Superconducting Coil", IEEE Trans on PAS, Vol. PAS-101, pp 3988-3996, Oct 1982

[9] M. Ramamoorthy, C. Nagamani, V.N. Nandakumar, R.K. Hegde and S. Nandi, "Analysis of an Unsymmetrically Fired Phase Controlled Rectifier used as a Static VAR Generator", IEEE, Ten-Con, Jan 1991

[10] Electric Power Research Institute (EPRI), Aug. 1987.

[11] R.K. Varma, "Control of Static VAR Systems for Improvement of Dynamic Stability and Damping of Torsional Oscillations", Ph.D. Thesis, Apr. 1988.

[12] L. Gyugyi, FIEE, "Unified Power Flow Control Concept for Flexible AC Transmission Systems", IEE Proc. - C, Vol. 139, No. 4, July 1992.

APPENDIX - A

VARIABLES

$$U_{11} = (n+1)\alpha - 150n + 60^\circ$$
$$U_{12} = U_{11} + 60n$$
$$U_{13} = U_{11} + 240n$$
$$U_{14} = U_{11} + 180n$$
$$U_{21} = (n+1)\alpha + 150n - 60^\circ$$
$$U_{22} = U_{21} - 60n$$
$$U_{23} = U_{21} - 240n$$
$$U_{24} = U_{21} - 180n$$
$$U_{31} = U_{21} + 120^\circ$$
$$U_{32} = U_{22} - 60n$$
$$U_{33} = U_{23} - 60n$$
$$U_{34} = U_{24} + 120^\circ$$

$$V_{11} = (n-1)\alpha - 150n - 60^\circ$$
$$V_{12} = V_{11} + 60n$$
$$V_{13} = V_{11} + 240n$$
$$V_{14} = V_{11} + 180n$$
$$V_{21} = (n-1)\alpha + 150n + 60^\circ$$
$$V_{22} = V_{21} - 60n$$
$$V_{23} = V_{21} - 240n$$
$$V_{24} = V_{21} - 180n$$
$$V_{31} = V_{21} - 120^\circ$$
$$V_{32} = V_{22} + 60n$$
$$V_{33} = V_{21} - 120n$$
$$V_{34} = V_{11} + 120^\circ$$

$$p_1 = 8\cos(30n)\sin(90n)\,[\,\cos(\alpha+60^\circ\cos(n(\alpha-30^\circ)) + \cos(\alpha-60^\circ) \times \cos(n(\alpha+30^\circ))$$

$$p_2 = 8\sin(30n)\cos(90n)\,[\,\cos(\alpha+60^\circ\sin(n(\alpha-30^\circ)) - \cos(\alpha-60^\circ) \times \sin(n(\alpha+30^\circ))$$

$$p_3 = -\frac{8}{n}\cos(\alpha+60^\circ)\sin(n(\alpha-120^\circ))\cos(60n)$$

$$p_4 = -\frac{8}{n}\cos(\alpha-60^\circ)\sin(n(\alpha-60^\circ))\cos(90n)$$

$$p_5 = -\frac{4}{n}\sin(n(\alpha-60^\circ))\,(\cos(60n)\cos(\alpha-60^\circ)-\cos(90n)\cos(\alpha+60^\circ))$$

$$p_6 = -\frac{4}{n}\sin(n(\alpha-60^\circ))\,(\sin(30n)\cos(\alpha-60^\circ)-\sin(90n)\cos(\alpha+60^\circ))$$

$$P_7 = -\sin U_{11} - \sin U_{12} + \sin U_{13} + \sin U_{14} + \sin U_{21} + \sin U_{22} - \sin U_{23} - \sin U_{24}$$

$$P_8 = -\sin V_{11} - \sin V_{12} + \sin V_{13} + \sin V_{14} + \sin V_{21} + \sin V_{22} - \sin V_{23} - \sin V_{24}$$

$$P_9 = -\cos U_{11} + \cos U_{12} + \cos U_{13} - \cos U_{14} - \cos U_{21} + \cos U_{22} + \cos U_{23} - \cos U_{24}$$

$$P_{10} = -\cos V_{11} + \cos V_{12} + \cos V_{13} - \cos V_{14} - \cos V_{21} + \cos V_{22} - \cos V_{23} - \cos V_{24}$$

$$P_{11} = -\cos U_{11} + \cos U_{12} - \cos U_{13} + \cos U_{14} + \cos U_{21} - \cos U_{22} + \cos U_{23} - \cos U_{24} + \cos U_{31} + \cos U_{32} - \cos U_{33} - \cos U_{34}$$

$$P_{12} = +\cos V_{11} - \cos V_{12} + \cos V_{13} - \cos V_{14} - \cos V_{21} + \cos V_{22} - \cos V_{23} + \cos V_{24} - \cos V_{31} + \cos V_{32} - \cos V_{33} + \cos V_{34}$$

$$P_{13} = +\sin U_{11} + \sin U_{12} + \sin U_{13} + \sin U_{14} + \sin U_{21} + \sin U_{22} + \sin U_{23} + \sin U_{24} + \sin U_{31} + \sin U_{32} + \sin U_{33} + \sin U_{34}$$

$$P_{14} = -\sin V_{11} - \sin V_{12} - \sin V_{13} - \sin V_{14} - \sin V_{21} - \sin V_{22} - \sin V_{23} - \sin V_{24} - \sin V_{31} - \sin V_{32} - \sin V_{33} - \sin V_{34}$$

$$P_{15} = + \sin U_{11} + \sin U_{12} + \sin U_{13} + \sin U_{14} + \sin U_{21} + \sin U_{22}$$
$$+ \sin U_{23} + \sin U_{24} + \sin U_{31} + \sin U_{32} + \sin U_{33} + \sin U_{34}$$

$$P_{16} = + \sin V_{11} + \sin V_{12} + \sin V_{13} + \sin V_{14} + \sin V_{21} + \sin V_{22}$$
$$+ \sin V_{23} + \sin V_{24} + \sin V_{31} + \sin V_{32} + \sin V_{33} + \sin V_{34}$$

$$P_{17} = + \cos U_{11} - \cos U_{12} + \cos U_{13} - \cos U_{14} - \cos U_{21} + \cos U_{22}$$
$$- \cos U_{23} + \cos U_{24} - \cos U_{31} - \cos U_{32} + \cos U_{33} + \cos U_{34}$$

$$P_{18} = + \cos V_{11} - \cos V_{12} + \cos V_{13} - \cos V_{14} - \cos V_{21} - \cos V_{22}$$
$$- \cos V_{23} + \cos V_{24} - \cos V_{31} + \cos V_{32} - \cos V_{33} + \cos V_{34}$$

APPENDIX - B

SYSTEM DATA

The system data is same as in [11]

Transmission line data

Resistance R = 0.055 Ω per phase per mile

Reactance X_L = 0.52 Ω per phase per mile

Susceptance ($B_C = 1/X_C$) = 5.92 μ mho per phase per mile

Controller data

$K = 200$, $T = 0.5$ sec.

$\alpha_{max} = 60^\circ$, $\alpha_{min} = 20^\circ$

Base quantities

Voltage = 230 kV

MVA = 100

Frequency = 50 Hz